AFRL-AFOSR-UK-TR-2022-0028

Integrated Guidance and Weapon Target Assignment (WTA) for Swarm Engagements

Shima, Tal
TECHNION ISRAEL INSTITUTE OF TECHNOLOGY
TECHNION CITY
HAIFA, , 32000
IL

03/09/2022
Final Technical Report

Air Force Research Laboratory
Air Force Office of Scientific Research
European Office of Aerospace Research and Development
Unit 4515 Box 14, APO AE 09421

REPORT DOCUMENTATION PAGE

PLEASE DO NOT RETURN YOUR FORM TO THE ABOVE ORGANIZATION.

1. REPORT DATE	2. REPORT TYPE	3. DATES COVERED	
20220309	Final	START DATE 20190915	END DATE 20210914

4. TITLE AND SUBTITLE
Integrated Guidance and Weapon Target Assignment (WTA) for Swarm Engagements

5a. CONTRACT NUMBER	5b. GRANT NUMBER	5c. PROGRAM ELEMENT NUMBER
	FA9550-19-1-7042	
5d. PROJECT NUMBER	**5e. TASK NUMBER**	**5f. WORK UNIT NUMBER**

6. AUTHOR(S)
Tal Shima

7. PERFORMING ORGANIZATION NAME(S) AND ADDRESS(ES)
TECHNION ISRAEL INSTITUTE OF TECHNOLOGY
TECHNION CITY
HAIFA 32000
IL

8. PERFORMING ORGANIZATION REPORT NUMBER

9. SPONSORING/MONITORING AGENCY NAME(S) AND ADDRESS(ES)	10. SPONSOR/MONITOR'S ACRONYM(S)	11. SPONSOR/MONITOR'S REPORT NUMBER(S)
EOARD UNIT 4515 APO AE 09421-4515	AFRL/AFOSR IOE	AFRL-AFOSR-UK-TR-2022-0028

12. DISTRIBUTION/AVAILABILITY STATEMENT
A Distribution Unlimited: PB Public Release

13. SUPPLEMENTARY NOTES

14. ABSTRACT
The research was directed at the development of new algorithms and guidance concepts for teams of interceptors in swarm-on-swarm engagements with a particular emphasis on the interplay between the guidance and the weapon target assignment (WTA) process. The goal was to design and study cooperative guidance algorithms that use to a greater extent the kinematic capabilities of the guided vehicles while increasing the flexibility of the WTA process. In view of these goals, the research focused on two directions related to the problem of coordinated attack. The first direction of research concentrated on the problem of achieving simultaneous attack using cooperative geometric guidance laws. The second, complimentary, direction of research concentrated on obtaining an optimal guidance law that is able of achieving impact at a given time moment, so as to enable simultaneous intercept by multiple vehicles. The successful accomplishment of the research goals were published in two journal articles "Consensus-based cooperative geometrical rules for simultaneous target interception", and "Minimum-effort impact-time control guidance using quadratic kinematics approximation"

15. SUBJECT TERMS

16. SECURITY CLASSIFICATION OF:			17. LIMITATION OF ABSTRACT	18. NUMBER OF PAGES
a. REPORT U	b. ABSTRACT U	c. THIS PAGE U	SAR	47

19a. NAME OF RESPONSIBLE PERSON	19b. PHONE NUMBER *(Include area code)*
MARK FRIEND	314-235-6292

Faculty of Aerospace Engineering
Technion - Israel Institute of Technology

Integrated Guidance and Weapon Target Assignment for Swarm Engagements

AFOSR Contract No. FA9550-19-1-7042

Technical Report
(Covering the period: 15 September 2019 - 14 September 2021)

Principal Investigator: Prof. Tal Shima

Summary

The research was directed at the development of new algorithms and guidance concepts for teams of interceptors in swarm-on-swarm engagements with a particular emphasis on the interplay between the guidance and the weapon target assignment (WTA) process. The goal is to design and study cooperative guidance algorithms that use to a greater extent the kinematic capabilities of the guided vehicles while increasing the flexibility of the WTA process. In view of these goals, the research has focused on two directions related to the problem of coordinated attack.

The first direction of research concentrated on the problem of achieving simultaneous attack using cooperative geometric guidance laws. This direction of research was pursued in joint work with my M.Sc. student, B. Zadka, my Ph.D. student R. Tsalik, and my postdoc Dr. T. Tripathy.

The second, complimentary, direction of research concentrated on obtaining an optimal guidance law that is able of achieving impact at a given time moment, so as to enable simultaneous intercept by multiple vehicles. This direction of research was pursued in joint work by my Ph.D. student G. Merkulov and Dr. M. Weiss.

The results of this two years research effort were summarized in the following published journal publications:

- Zadka, B., Tripathy, T., Tsalik, R., and Shima, T., Consensus-based cooperative geometrical rules for simultaneous target interception, *Journal of Guidance, Control, and Dynamics*, Vol. 43, No. 12, 2020, pp. 2425–2432.
- Merkulov, G., Weiss, M., and Shima, T., Minimum-effort impact-time control guidance using quadratic kinematics approximation, *Journal of Guidance, Control, and Dynamics*, 2021, pp. 1–14.

Contents

List of Figures

I. Introduction

This research was aimed at developing new algorithms and guidance concepts for teams of interceptors in swarm-on-swarm engagements with a particular emphasis on the interplay between the guidance and the WTA process. To fix the ideas, we adopted a scenario that we used to motivate our problem formulation and to apply our research results. Throughout the investigation, we concentrated on the mid-course and end-game stages of the engagements assuming perfect information regarding all the states of the participants and we considered the problem from the point of view of the interceptor team.

One of the outstanding problems related to cooperative guidance is the problem of coordinated attack in which a group of interceptors tries to arrive at the same target at the same time, or at carefully planned moments of time. There are two main directions of research that we followed in order to tackle this problem.

The first direction of research consisted in devising geometric guidance rules that allow for efficient coordination between a possibly large number of coordinating interceptors. Using the tools of cyclic and leader-follower information exchange frameworks from multi-agent systems theory, we proposed cooperative geometrical rules and corresponding guidance laws to achieve simultaneous target interception at the minimum possible time and any desired impact time greater than the minimum, respectively. In the minimum impact time case, we proved that the impact time of each pursuer is guaranteed to converge to the maximum impact time among the pursuers in the case that they are heading straight to the target, resulting in a situation that is called max-consensus. For the case of desired impact time, the leader imposes the desired impact time independent of the other pursuers in the system, and the followers modify their impact times according to that of the leader, eventually leading to the simultaneous interception. Based on the cyclic and leader-follower frameworks, we present the geometrical rules and show that, by using them, we achieve simultaneous interception from arbitrary initial positions of the pursuers. The corresponding guidance laws were implemented using a Proportional Integral controller.

The second direction of research was aimed at deriving an optimal guidance law that achieves a desired impact time while optimizing a quadratic guidance effort criterion. This part of the work relates to the classical one-on-one intercept problem, but provides a tool that is very useful for building efficient many-on-many guidance solutions. Technically, it presents the solution to the problem of minimum integral guidance effort control for an approximate second-order kinematic vehicle. The advantage of using the approximate second-order kinematics is that it allows to develop "analytic" solutions, that is a closed loop solution that can be realistically implemented on a guidance computer as it is based on simple algebraic computations and one-dimensional look-up tables. An additional aspect of the solution that we obtained is that it allows very simple and quite accurate estimates of the optimal guidance effort and the maximum lateral acceleration that is necessary to realize it. These estimates are of great importance in obtaining effective many-on-many intercept guidance strategies, as they allow for solving complicated weapon target allocation problems while taking into account guidance performance of underlying interceptors and their individual limitations in terms of maximum lateral acceleration.

The remaining part of this report has two sections, presenting in detail the research performed in each of the above two directions.

In the next section, we present new cooperative guidance laws to achieve simultaneous interception of a stationary target by a team of n heterogeneous pursuers, modelled with non-linear unicycle kinematics. The proposed laws implement a max-consensus protocol to achieve simultaneous target interception where consensus is achieved in the impact times of the pursuers. The interception can occur either in the minimum possible time or in any desired impact time which is greater than the minimum possible time. To achieve the former, we propose a guidance law for each pursuer using a cyclic pursuit framework wherein the pursuer requires the position and speed information pertaining to itself and its neighbour only. For a desired impact time, we propose another guidance law using a leader-follower framework, in which the leader imposes the desired impact time using a suitable circular trajectory. The other pursuers adjust their trajectories with respect to the leader, eventually leading to simultaneous interception in the desired impact time. The proposed guidance laws are designed using PI controllers in order to eliminate any deviations from the desired trajectories. Each guidance law is studied in various scenarios through non-linear simulations, showing that simultaneous interception of the target is achieved in the specified impact time from arbitrary initial positions of the pursuers. The results of this effort were recently published in the AIAA Journal of Guidance, Control, and Dynamics [1].

The following section, a guidance law for intercepting a stationary target is derived based on solving the minimum effort optimal control problem with fixed time and a quadratic approximation of the kinematic

equations. It is proven that this optimal control problem has, in general, a unique solution. Based on this solution, a guidance law is proposed that is shown to be implementable based on typically available sensor data, using a semi-analytic procedure. Numerical simulations show that the solution based on the second-order approximate kinematics matches closely the solution based on the original nonlinear kinematics that can only be obtained by numerical optimization. The results of this effort were recently published in the AIAA Journal of Guidance, Control, and Dynamics [2].

It should be noted that as this report is based on two different papers (mentioned above), there may be differences between the sections in some of the definitions and notations.

II. Consensus-based Cooperative Guidance Laws for Simultaneous Target Interception

Nomenclature

P_i	=	i^{th} pursuer
a_i	=	lateral acceleration of P_i, m/sec^2
Δt_i	=	time to reach the target for P_i, sec
d_i	=	difference parameter of P_i, sec
ϵ_i	=	look-angle of P_i, rad
ϵ_i^d	=	desired look-angle for P_i, rad
$\Delta\epsilon_i$	=	look-angle error for P_i, rad
γ_i	=	heading angle of P_i, rad
K_1	=	proportional gain
K_2	=	integral gain
λ_i	=	line-of-sight angle between P_i and the target, rad
L_i	=	arc length of a circle between P_i and the target, m
n	=	number of pursuers in the system
r_i	=	distance of P_i from the target, m
R_i	=	radius of a circle that P_i follows, m
t_d	=	desired impact time, sec
$\tilde{t}_i$	=	minimum impact time for P_i, sec
T	=	target
v_i	=	speed of P_i, m/sec
(x_i, y_i)	=	position coordinates of P_i in cartesian coordinate system, (m, m)

A. Scenario and problem formulation

A Multi-Agent System (MAS) consists of a number of pursuers, which interact with each other in a centralized or a de-centralized manner. The major challenge in the research of MAS is designing the interaction rules and control inputs to ensure that a desired task is achieved collectively. Common tasks fulfilled by such systems are obtaining a desired formation between the pursuers, reaching consensus upon a desired parameter, or leading the pursuers to a rendezvous point. The kinematics of the pursuers are usually described by models like single integrator, double integrator, or unicycle. In our work, we will focus on solving the rendezvous problem at a pre-specified target point using pursuers modelled as unicycles, which are non-linear vehicles that can be controlled using angular and translational speeds. The choice of unicycle kinematics is owing to the fact that such kinematics can be used to represent simplified models of systems like missiles, cars, robots, *etc.*

The problem of guiding a single missile to impact a target at a desired time has been investigated extensively in the literature. In one of the earliest works in this area [3], Jeon *et al.* presented an impact time control guidance law which combined proportional navigation guidance (PNG) law with a feedback on the impact time error to achieve a pre-defined impact time for the missile. Sliding mode control based guidance laws, as proposed by Kumar and Ghose [4] and Cho and Kim [5], has also been used to control the impact time by incorporating the error between the desired impact time and the estimated time-to-go in the sliding surface. Saleem and Ratnoo [6] proposed a Lyapunov-based guidance law to control the impact time by modification of the heading error, where the selection of the desired impact time was limited by the initial conditions of the scenario. Controlling the impact-time via polynomial look-angle shaping was proposed by Tekin *et al.* for stationary targets [7] and varying speed targets [8]. In these papers, the authors proposed quadratic and cubic shaping, where the cubic shaping showed results similar to the optimal results. In a recent work [9], Tsalik and Shima proposed a circular impact time guidance law to achieve a desired impact time for a stationary or a non-maneuvering moving target. The desired impact time was achieved by constraining the pursuer to move in a suitable circular trajectory.

One of the popular information exchange topologies which has been used to implement consensus protocols in MAS is the cyclic pursuit framework. In this framework, pursuer i receives information from the $i+1$ modulo n pursuer. Borrowed from the natural behaviour of animals such as dogs, birds, and ants, the advantage of this framework is its simplicity and the minimum sensor information requirement. An illustration of the information exchange topology in the cyclic pursuit framework is presented in Fig. 1.

Considering the rendezvous problem, the cyclic pursuit for pursuers with single integrator kinematics was studied in [10] by Bruckstein *et al.* and was extended to unicycle kinematics by Marshall *et al.* [11]. For unicycle kinematics, cyclic pursuit has also been used to address problems such as area surveillance [12], formation control of homogeneous [13] and heterogeneous [14] pursuers, *etc.* In a recent work, Kumar and Mukherjee [15] proposed a cooperative guidance law in a cyclic pursuit framework to solve the simultaneous target interception problem by a team of pursuers by achieving consensus in the time-to-go of the pursuers.

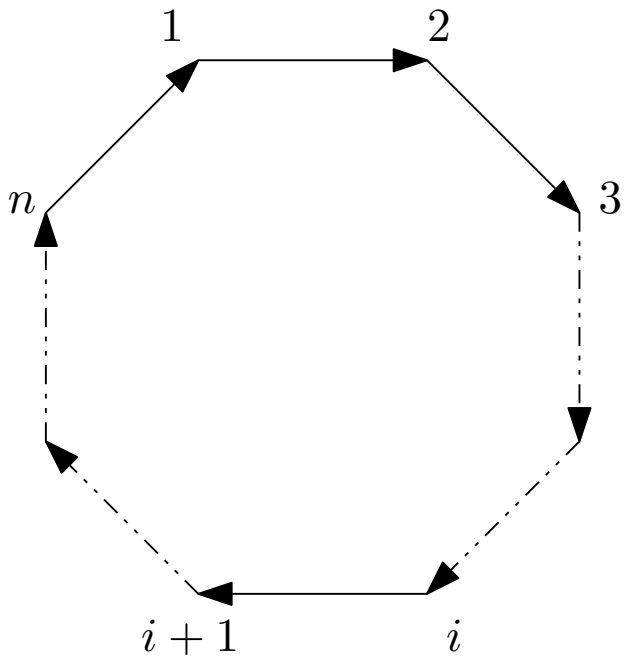

Figure 1: Information Exchange in cyclic pursuit framework.

The leader-follower framework is another information exchange topology which is commonly used in the MAS literature. In this framework, the pursuers in the system are divided into distinct groups of leaders and followers. The leaders' behaviour is usually independent of the other members in the group, whereas the followers are dependent on information received by the leader.

Jadbabaie *et al.* proved in [16] that the followers converge to the leader as long as all of the members in the group are linked to the leader, not necessarily in a direct way. Leader-follower consensus problems were also studied for the cases where time-delays are present and the communication topology is switching for agents with second order dynamics in [17],[18]. The formation control problem has also been studied under the leader-follower framework in [19] and [20] for autonomous agents with unicycle dynamics. An extension to the missile guidance area for missiles with unicycle dynamics was proposed by Sun *et al.* [21], where the authors designed a cooperative guidance law by feedback linearization such that the impact time of each follower converges to the impact time of the leader in finite time.

Using the tools of cyclic pursuit and leader-follower frameworks from MAS, here we propose cooperative guidance laws to achieve simultaneous target interception in the minimum possible impact time or in any greater desired impact time. In the present framework, the target is assumed to be stationary, which could represent a given landmark, a beacon, *etc.* The pursuers are modelled with unicycle kinematics and have different linear speeds, which makes the system heterogeneous. The underlying idea is that if each pursuer adjusts its trajectory according to the impact time of its neighbour as if that neighbour heads straight to the target, then consensus will eventually be achieved in the impact times of all the pursuers. In the minimum possible impact time case, the information exchange topology follows a cyclic pursuit framework. The impact

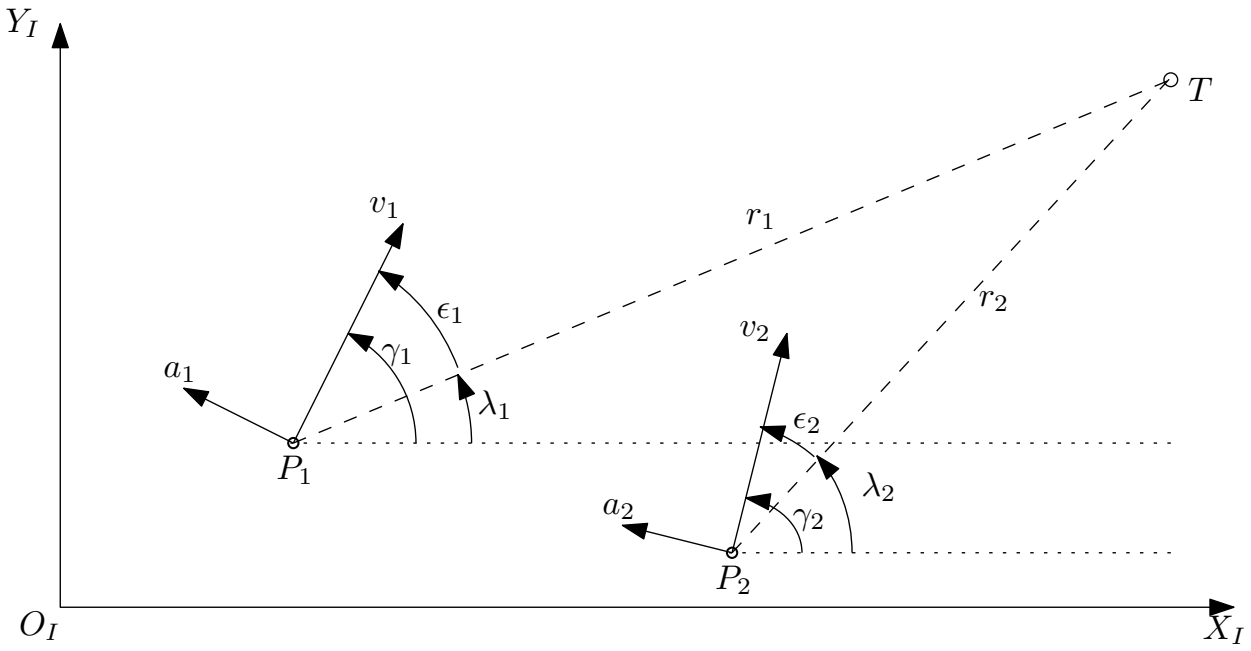

Figure 2: Planar engagement.

time of each pursuer in the group is guaranteed to converge to the impact time of the pursuer which has the largest initial impact time resulting in max-consensus.

We address the problem of simultaneous interception of a target by a group of n pursuers in finite time. The pursuers are modelled as unicycles and have constant linear speeds. The target is assumed to be stationary and represents any point of interest like a landmark or a beacon. Fig. 2 presents a schematic view of the planar geometry between the target and the pursuers. The $X_I - O_I - Y_I$ axes form a Cartesian inertial reference frame. The position coordinates of the target T are given by $(x_T, y_T) \in \mathbb{R}^2$. For every $i \in \{1, 2, .., n\}$, the i^{th} pursuer is denoted by P_i and its position coordinates by $(x_i, y_i) \in \mathbb{R}^2$. Its linear speed, heading angle, and normal acceleration are written as v_i, γ_i, and a_i, respectively. The equations of motion of pursuer P_i are as given below,

$$\begin{aligned} \dot{x}_i &= v_i \cos\gamma_i \\ \dot{y}_i &= v_i \sin\gamma_i \\ \dot{\gamma}_i &= \frac{a_i}{v_i} \end{aligned} \tag{1}$$

The pursuers are assumed to be heterogeneous in terms of their speed which can be different for all the pursuers. The distance and the line-of-sight (LOS) angle between P_i and the target are denoted by r_i and λ_i, respectively. ϵ_i is referred to as the look-angle, which is defined as the angle between the velocity vector of P_i and its corresponding LOS to the target. The equations of motion of P_i can also be expressed in a polar coordinate frame attached to the pursuer, as follows,

$$\begin{aligned} \dot{r}_i &= -v_i \cos\epsilon_i \\ \dot{\lambda}_i &= -\frac{v_i \sin\epsilon_i}{r_i} \\ \dot{\gamma}_i &= \frac{a_i}{v_i} \end{aligned} \tag{2}$$

The main objective of this work is to propose cooperative guidance laws which lead to simultaneous target interception by the n pursuers. In the next section, we explore some concepts from MAS to achieve the goal.

B. Consensus Protocols for Simultaneous Target Interception

In this section, we propose geometrical rules that lead to the simultaneous interception of a stationary target by a group of n heterogeneous pursuers. Our goal is to control the impact time of the pursuers by using consensus protocols that will lead to consensus in the impact times of the pursuers, therefore achieving simultaneous interception of the target. We propose two kinds of geometrical rules which drive the system towards the target while achieving either the minimum possible impact time or any desired impact time which is greater than the minimum possible time.

1. A Cyclic Pursuit Strategy to Achieve a Minimum Impact Time

Here, we present a geometrical rule that leads to simultaneous interception of the target in the minimum possible time. It can be achieved by synchronizing the impact times of the pursuers, so the impact time is chosen as the consensus parameter. Then, simultaneous target interception is guaranteed if consensus is achieved.

Now, let us define the following parameter,

$$\tilde{t}_i(t) = \frac{r_i(t)}{v_i} \tag{3}$$

which is the time required for P_i to reach the target if it follows a straight-line trajectory towards the target. Therefore, $\tilde{t}_i(t)$ is the minimum possible value of the impact time of P_i at any given time t. We choose $\tilde{t}_i$ as the consensus parameter since as time propagates, synchronizing this parameter implies simultaneous interception in the minimum possible time. When a pursuer follows any trajectory other than a straight line, the computation of the impact time might not be always straightforward and is then derived by estimations which are prone to errors. Considering this, $\tilde{t}_i$ is the suitable consensus parameter as it is dependent on position and speed measurements which are easier to derive.

We consider a cyclic pursuit based information exchange topology among the pursuers, so the guidance law for P_i is based on the information of only its neighbour P_{i+1}. In order to achieve consensus, we propose that each pursuer compares its $\tilde{t}_i$ with that of its neighbour and adjusts its trajectory accordingly to synchronise its impact time with that of its neighbour.

Remark 1. *Note that for any P_i, $\tilde{t}_i$ can be controlled by modifying its trajectory. Then, as long as we can suitably modify the parameters governing its trajectory while controlling $\tilde{t}_i$, each pursuer can follow any trajectory.*

It is clear from Remark 1 that any trajectory that allows us to control $\tilde{t}_i$ for every $i \in \{1, 2, .., n\}$ can be used to implement the proposed consensus protocol. In this work, we propose to use circular trajectories for all the pursuers. The choice of circular trajectories is owing to the fact that the impact times to the target can be easily controlled in this case which has been shown by Tsalik and Shima in [9]. The authors prove that by controlling the curvature of the circular trajectory of P_i, we can directly control the length of its trajectory and accordingly its impact time and $\tilde{t}_i$.

For the circular trajectory shown in Fig. 3, the radius of the circle can be expressed as $R_i = \frac{r_i}{2\sin\epsilon_i}$. Then the arc length of the circle between P_i and the target is $L_i = 2\epsilon_i R_i = r_i\epsilon_i/\sin\epsilon_i$. Since the linear speed is assumed to be constant, $L_i = v_i\Delta t_i$, where Δt_i is the time in which P_i will reach the target. By combining these two expressions for L_i, it directly follows that,

$$\epsilon_i = \text{Asinc}\left(\frac{r_i}{v_i\Delta t_i}\right) = \text{Asinc}\left(\frac{\tilde{t}_i}{\Delta t_i}\right) \tag{4}$$

where the Asinc function is the inverse function of the sinc function, defined as $\text{sinc}(\epsilon) = \frac{\sin(\epsilon)}{\epsilon}$. By controlling the look-angle ϵ_i of P_i, its impact time to the target Δt_i can be directly controlled and *vice versa*.

Now, in the present cyclic pursuit framework, each pursuer follows a circular trajectory while trying to synchronize its impact time with that of its neighbour. The communication between the pursuers and the obtained trajectories are illustrated in Fig. 4. As discussed before, the minimum impact time to the target for P_i is $\tilde{t}_i$. Since we are interested in achieving simultaneous target interception in minimum time, we try to achieve consensus in $\tilde{t}_i$s. In order to synchronize $\tilde{t}_i s,\ i \in \{1, 2, .., n\}$, P_i modifies its trajectory based on the relation between its $\tilde{t}_i$ and that of its neighbour $\tilde{t}_{i+1}$ as explained below:

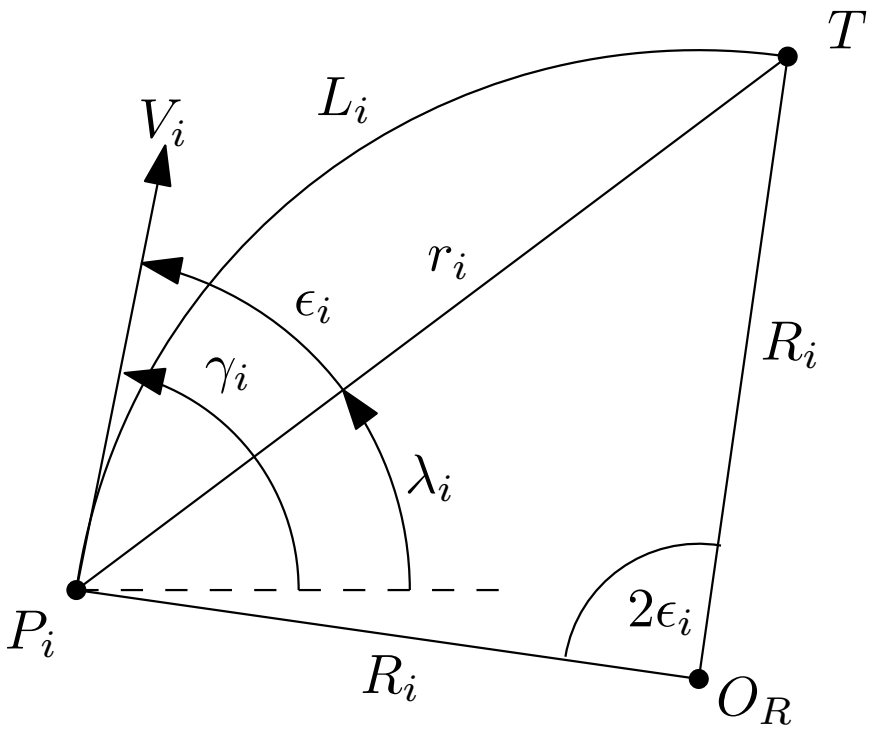

Figure 3: Circular trajectory geometry

- $\tilde{t}_i \leq \tilde{t}_{i+1}$: In this case, we set the desired impact time of P_i to the time that its neighbour requires to arrive at the target in a straight line, implying $\Delta t_i = \tilde{t}_{i+1}$. Substituting this in Eq. Eq. (4), we get the corresponding value of the look-angle ϵ_i. Then, P_i modifies its look-angle accordingly to generate a circular trajectory with a longer arc to the target. This increases the time it takes to reach the target while synchronizing its impact time with that of its neighbour.
- $\tilde{t}_i > \tilde{t}_{i+1}$: Here, P_i tries to reach the target as fast as it can. Hence, it nullifies its look-angle and heads straight to the target.

Based on this logic, the geometrical rule can be expressed mathematically as given below,

$$\epsilon_i = \begin{cases} \text{Asinc}(\tilde{t}_i/\tilde{t}_{i+1}) & \tilde{t}_i \leq \tilde{t}_{i+1} \\ 0 & \tilde{t}_i > \tilde{t}_{i+1} \end{cases} \tag{5}$$

By following this geometrical rule, P_i adjusts its trajectory according to its neighbour, when $\tilde{t}_{i+1} \geq \tilde{t}_i$. Therefore, eventually the impact time $\tilde{t}_i$ of P_i converges to $\max_{i \in \mathbb{N}_n}(\tilde{t}_i)$ of the group leading to max-consensus. Once consensus is achieved, all the pursuers synchronise their impact times and reach the target simultaneously. The proof that the system converges to $\max_{i \in \mathbb{N}_n}(\tilde{t}_i)$ leading to simultaneous interception is outlined herein.

Theorem 1. Consider n pursuers with unicycle kinematics in a cyclic pursuit framework. The trajectories of the pursuers are governed by the geometrical rule described in Eq. Eq. (5). Simultaneous interception of any pre-specified target point is guaranteed from arbitrary initial positions of the pursuers by achieving max-consensus in their impact times to the target. Moreover, interception is achieved in the minimum possible time, which is equal to the maximum impact time among the pursuers in the case that they are heading straight to the target.

Proof. : Without any loss of generality, let us assume that $\tilde{t}_1(0) \neq \tilde{t}_2(0) \neq ... \neq \tilde{t}_n(0)$. Then, we denote P_k as the unique pursuer which satisfies the condition $\tilde{t}_k(0) = \max_{i \in \mathbb{N}_n}[\tilde{t}_i(0)]$. This leads us to define a difference

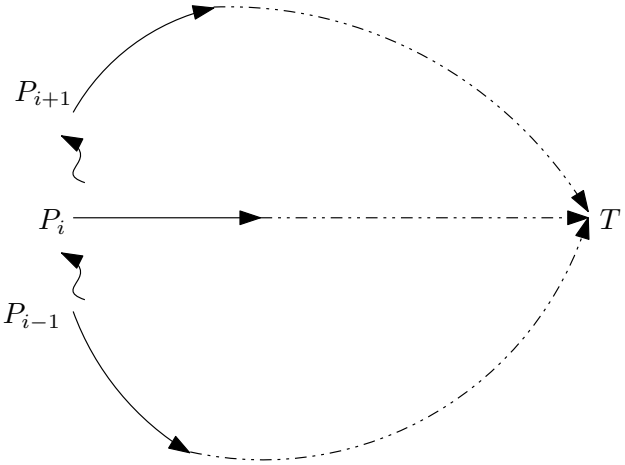

Figure 4: Interception at minimum time.

function for every P_i as

$$d_i(t) \equiv \tilde{t}_k(t) - \tilde{t}_i(t). \tag{6}$$

Now we first prove that $\tilde{t}_k(t)$ remains maximum for all $t > 0$, equivalently $\tilde{t}_k(t) = \max_{i \in \mathbb{N}_n} \big[\tilde{t}_i(t)\big]\ \forall t$. By definition, $\tilde{t}_{k-1}(0) < \tilde{t}_k(0)$ and $d_{k-1}(0) > 0$ for P_{k-1}. Let us assume there exists time $t = t^*$ at which $d_{k-1}(t^*) < 0$. For every i, $\dot{d}_i(t) = -\cos\epsilon_k(t) + \cos\epsilon_i(t)$ is bounded implying that $d_i(t)$ is continuous [22]. Applying intermediate value theorem, there exists a time $t^\dagger < t^*$ at which $d_{k-1}(t^\dagger) = 0$ and $\tilde{t}_{k-1}(t^\dagger) = \tilde{t}_k(t^\dagger)$. Then, $\epsilon_{k-1}(t^\dagger) = 0$ according to Eq. Eq. (5) and $\dot{d}_{k-1}(t^\dagger) = -\cos\epsilon_k(t^\dagger) + 1 \geq 0$ using Eq. Eq. (2). This implies that $d_{k-1}(t) \geq 0$ for $t \geq t^\dagger$ which contradicts the assumption that $d_{k-1}(t^*) < 0$. Therefore, $d_{k-1}(t) \geq 0$ and $\tilde{t}_{k-1}(t) \leq \tilde{t}_k(t)\ \forall t \geq 0$.

Next, we analyse the behaviour of P_{k-2}. Two cases arise, $\tilde{t}_{k-2}(0) < \tilde{t}_{k-1}(0)$ or $\tilde{t}_{k-2}(0) > \tilde{t}_{k-1}(0)$. When $\tilde{t}_{k-2}(0) < \tilde{t}_{k-1}(0)$, using the preceding analysis we know that $\tilde{t}_{k-2}(t) \leq \tilde{t}_{k-1}(t)$, hence, $\tilde{t}_{k-2}(t) \leq \tilde{t}_k(t)$ throughout the engagement. For $\tilde{t}_{k-2}(0) > \tilde{t}_{k-1}(0)$, using Eqs. Eq. (2), Eq. (5) and Eq. (6), we get $\epsilon_{k-2}(0) = 0$, $\dot{d}_{k-2}(0) = -\cos\epsilon_k(t) + 1 \geq 0$ and $d_{k-2}(0) > 0$. Now, let us assume there exists a time at which $d_{k-2}(t)$ changes sign. Applying intermediate value theorem, then there exists a time t^* at which $d_{k-2}(t^*) = 0$. Since $d_{k-2}(0) > 0$ there has to be $t^\dagger < t^*$ at which $\dot{d}_{k-2}(t^\dagger) = -\cos\epsilon_k(t^\dagger) + \cos\epsilon_{k-2}(t^\dagger) < 0$ which is possible when $\epsilon_{k-2}(t^\dagger) \neq 0$. According to Eq. Eq. (5), this will occur only if $\tilde{t}_{k-2}(t^\dagger) \leq \tilde{t}_{k-1}(t^\dagger)$. Similar to the first case, then $\tilde{t}_{k-2}(t) \leq \tilde{t}_{k-1}(t)$, $\tilde{t}_{k-2}(t) \leq \tilde{t}_k(t)$ and $d_{k-2}(t) \geq 0\ \forall t \geq t^\dagger$, which contradicts our assumption of sign change of $d_{k-2}(t)$. Hence, $d_{k-2}(t) \geq 0$ and $\tilde{t}_{k-2}(t) \leq \tilde{t}_k(t)\ \forall t > 0$. Continuing in the same lines for the rest of the pursuers, it can be shown that $\tilde{t}_k(t) = \max_{i \in \mathbb{N}_n} \big[\tilde{t}_i(t)\big]\ \forall t > 0$.

Now we will show that target interception occurs simultaneously at $t = \tilde{t}_k(0)$. We already know that $\tilde{t}_k(t) = \max_{i \in \mathbb{N}_n} \big[\tilde{t}_i(t)\big]\ \forall t$. Using this condition in Eq. Eq. (5), we get $\epsilon_k(t) = 0\ \forall t$ which means that P_k moves in a straight line to the target. Therefore, $\tilde{t}_k(t) = \tilde{t}_k(0) - t$ and P_k intercepts the target at $t = \tilde{t}_k(0)$. Let us assume that P_{k-1} intercepts the target at $t^* < \tilde{t}_k(0)$, then $\tilde{t}_{k-1}(t^*) = 0$ and $r_{k-1}(t^*) = 0$. Since $\tilde{t}_k(t^*) > 0$, Eq. Eq. (5) gives $\epsilon_{k-1}(t^*) = \text{Asinc}(0) = \pi$. Since $\epsilon_{k-1}(t)$ is a continuous function, there exists δ_t, in which $\frac{\pi}{2} < \epsilon_{k-1}(t) < \frac{3\pi}{2}\ \forall t \in (t^* - \delta_t, t^*]$. This implies $\dot{r}_{k-1}(t) > 0$ in this interval, hence P_{k-1} moves away from the target. This contradicts the assumption of existence of $t^* < \tilde{t}_k(0)$ at which $r_{k-1}(t^*) = 0$. So let us consider the scenario when $t^* > \tilde{t}_k(0)$. Then $\tilde{t}_{k-1} > \tilde{t}_k$ at $t = \tilde{t}_k(0)$ which is not possible as proved in the first half of the proof. Hence, the only possibility is $t^* = \tilde{t}_k(0)$. By applying this analysis for the rest of the pursuers in the system, it follows directly that all of them intercept the target simultaneously at $t = \tilde{t}_k(0)$ as desired. The assumption of unique $\tilde{t}_i(0)$s was for simplicity, the proof can be easily extended to the cases when $\tilde{t}_i(0)$s are not unique. □

In conclusion, the group of pursuers converge to the impact time of the pursuer with the maximum value of the initial $\tilde{t}_i$, thereby leading to max-consensus. It is also important to note that convergence is guaranteed for every possible initial positions of the pursuers.

Corollary 1. Given pursuer P_k that heads straight to the target, the trajectory of pursuer P_{k-1} is circular.

Proof. : As mentioned in the proof of Theorem 1, $\tilde{t}_k(t) = \max_{i \in \mathbb{N}_n} \left(\tilde{t}_i(t)\right)\ \forall t \in [0, \tilde{t}_k(0)]$, which leads to $\tilde{t}_{k-1}(0) < \tilde{t}_k(0)$. Using Eq. Eq. (5), we obtain,

$$\epsilon_{k-1} = \text{Asinc}\left(\frac{\tilde{t}_{k-1}}{\tilde{t}_k}\right) = \text{Asinc}\left(\frac{\tilde{t}_{k-1}}{\tilde{t}_k(0) - t}\right) \tag{7}$$

By using the work presented in [9], we know that Eq. Eq. (7) represents a geometrical rule that leads to a circular trajectory. Hence, the trajectory of pursuer P_{k-1} is circular. □

Having proved the convergence properties of the geometrical rule given in Eq. Eq. (5), we will now propose another geometrical rule for imposing a desired impact time.

2. Leader-Follower Strategy to Achieve a Desired Impact Time

Adjusting the impact time, and particularly enlarging it can be useful in cases where we want to increase the time for better decision making. In this section, we propose to use a leader-follower strategy to achieve a desired impact time which can be greater than the minimum possible impact time. We choose one any of the pursuers as the leader and denote it as P_0, and force it to impose a circular trajectory with a given desired time independent of the other pursuers in the system. The rest of the pursuers in the system, called the followers, communicate with the group using either an n-to-one or a one-to-one communication topology which are defined below.

Definition 1. n-to-one communication topology: In this case, for $i \in \{1, ..., n-1\}$, every pursuer P_i modifies its trajectory with respect to the information transferred from the leader P_0 as shown in Fig. 5a.

Definition 2. One-to-one communication topology: Here, for $i \in \{1, ..., n-1\}$, every pursuer P_i modifies its trajectory with respect to the information transferred from pursuer P_{i+1} except pursuer P_{n-1} which receives its information from the leader P_0. The information flow is depicted in Fig. 5b.

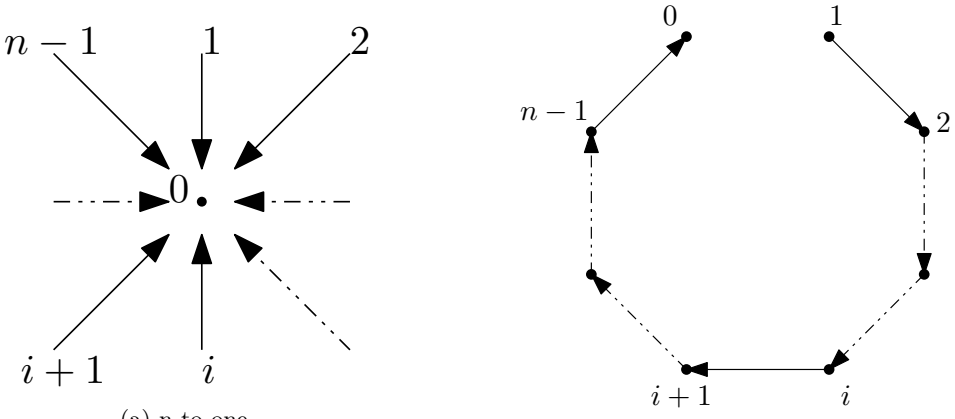

(a) n-to-one.

(b) one-to-one.

Figure 5: Leader-follower communication topology

A choice between the two communication topologies depends on the sensing capabilities of the system. The one-to-one topology should be used when the leader cannot communicate with all of the pursuers owing to sensing limitations, and the followers can communicate with each other. On the contrary, the n-to-one topology should be used in cases where the leader is able to transmit information to all the pursuers.

Now, we propose the geometrical rule for each of the two communication topologies. Note that in both cases, P_0 can be chosen arbitrarily as any one of the pursuers, where the choice has to be done a priori and cannot be changed during the engagement. For the n-to-one topology, the leader modifies its impact time by elongating its trajectory with respect to the desired impact time. This is done by using Eq. Eq. (4) for the leader P_0 and replacing Δt_i with $t_d - t$, where t_d is the desired impact time. Note that $t_d - t$ represents the time to go with respect to the desired impact time. The followers modify their impact time by elongating

their trajectories with respect to the leader, which is achieved by replacing Δt_i with $\tilde{t}_0$ in Eq. Eq. (4). The geometrical rule can then be expressed mathematically as given below,

$$\epsilon_0 = \text{Asinc}\left(\frac{\tilde{t}_0}{t_d - t}\right)$$
$$\epsilon_i = \begin{cases} \text{Asinc}\left(\frac{\tilde{t}_i}{\tilde{t}_0}\right) & \tilde{t}_i \leq \tilde{t}_0 \\ 0 & \tilde{t}_i > \tilde{t}_0 \end{cases} i = 1, 2, ..., n-1 \tag{8}$$

For the one-to-one topology, the leader modifies its impact time in the same way described for the n-to-one communication topology. However, instead of referring to the leader P_0, the followers refer to their neighbours. So, each follower P_i modifies its impact time by elongating its trajectory with respect to pursuer P_{i+1} by replacing Δt_i with $\tilde{t}_{i+1}$ in Eq. Eq. (4). The geometrical rule can then be expressed mathematically as,

$$\epsilon_0 = \text{Asinc}\left(\frac{\tilde{t}_0}{t_d - t}\right)$$
$$\epsilon_i = \begin{cases} \text{Asinc}\left(\frac{\tilde{t}_i}{\tilde{t}_{i+1}}\right) & \tilde{t}_i \leq \tilde{t}_{i+1} \\ 0 & \tilde{t}_i > \tilde{t}_{i+1} \end{cases} i = 1, 2, ..., n-1 \tag{9}$$

Note that t_d is greater than the minimum possible impact time. However, simultaneous target interception still occurs which is shown in the following theorem,

Theorem 2. Consider n pursuers modelled with unicycle kinematics and located at arbitrary initial positions, trying to intercept a stationary target in a desired impact time t_d which satisfies the following condition,

$$t_d > \max_{i \in \mathbb{N}_n} \left(\tilde{t}_i|_{t=0}\right).$$

Simultaneous interception of the target in time t_d is always guaranteed by following the geometrical rule given in either Eq. Eq. (8) or Eq. (9), where the underlying communication topology between the pursuers is either n-to-one or one-to-one, respectively.

Proof. : To begin with, we consider the n-to-one leader-follower communication topology. As mentioned before, the leader P_0 can be chosen arbitrarily as any one of the pursuers. Let us define a virtual pursuer P_v such that $\tilde{t}_v|_{t=0} = t_d > \max_{i \in \mathbb{N}_n} \left(\tilde{t}_i|_{t=0}\right)$. Let us consider any follower P_i where $i \in \{1, 2, .., n-1\}$. In an n-to-one topology, every P_i receives information solely from P_0, irrespective of the other pursuers in the system. Now, consider the sub-system consisting of pursuer P_i, leader P_0, and the virtual pursuer P_v in a cyclic pursuit framework. Here, P_i receives information from P_0, P_0 from P_v and P_v from P_i while following the geometrical rule in Eq. Eq. (5).

From the proof of Theorem 1, we know that the pursuer which heads straight to the target initially, keeps going straight. So, P_v moves in a straight line as $\tilde{t}_v(t) = \max\{\tilde{t}_i(t), \tilde{t}_0(t), \tilde{t}_v(t)\} \forall t \in [0, t_d]$. For the leader P_0, we get $\Delta t_0(t) = \tilde{t}_v(t) = t_d - t$ as $\tilde{t}_0(t) < \tilde{t}_v(t)$ and it follows a circular trajectory according to Corollary 1. As P_i adjusts its trajectory with respect to P_0, we get $\Delta t_i = \tilde{t}_0$. Substituting these in Eq. Eq. (5), we get the geometrical rule given in Eq. Eq. (8). Now, from Theorem 1, we know that the geometrical rule leads to simultaneous target interception by the sub-system in time t_d. Since the choice of i is arbitrary, the proof holds for every $i \in \{1, 2, .., n-1\}$.

For the one-to-one case as well, we introduce the virtual pursuer P_v which is defined exactly as the previous case. Now, we consider the system consisting of the $n-1$ followers, the leader P_0, and the virtual pursuer P_v in a cyclic pursuit framework. The rest of the analysis goes along the same lines as that for the n-to-one case which eventually guarantees simultaneous target interception in the desired time t_d under the geometrical rule given in Eq. Eq. (9). □

To conclude, we have proven that simultaneous interception in a desired impact time can be achieved in two different communication topologies by using a suitable geometrical rule. Moreover, the interception is guaranteed from any initial positions of the pursuers.

After deriving the geometrical rules, we will now design corresponding guidance laws and investigate their ability to provide simultaneous interception while handling heading errors and constrained look-angles.

C. Guidance Laws Design

In this subsection, we design guidance laws to enforce the geometrical rules obtained in the previous subsection. By enforcing the the geometrical rule, the desired look-angle is dictated for each pursuer in the system. The goal of the guidance laws, illustrated in Fig. 6, is to eliminate the look-angle deviations from the desired trajectories.

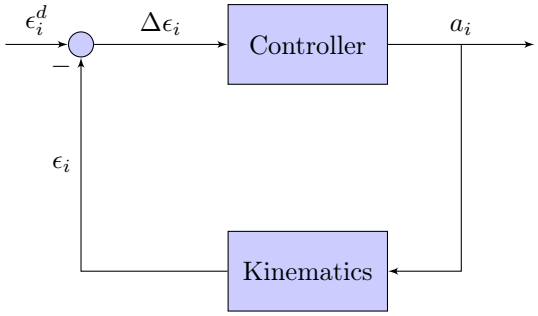

Figure 6: Control scheme

The look-angle error, $\Delta\epsilon_i$, is obtained as the difference between the desired look-angle, denoted as ϵ_i^d, and the current look-angle, ϵ_i. The value of ϵ_i^d is obtained from the geometrical rule, whereas ϵ_i is calculated from the kinematics equations. The error in the look-angle is fed into a PI controller to obtain the control input,

$$a_i = K_1\Delta\epsilon_i + \frac{K_2\Delta\epsilon_i}{s} \tag{10}$$

where K_1 is the proportional gain, which determines the ratio of output response to the error signal, and K_2 is the integral gain. The integral term sums the error over time, thus driving the steady-state error to zero. Note that the value of ϵ_i^d is different for each of the geometrical rules obtained in the previous subsection. Therefore, we obtain a correspondingly different guidance law for each one of them. Using the kinematics shown in Eq. Eq. (1), we derive γ_i. In the next step, we calculate the LOS angle by $\lambda_i = \arctan\left(\frac{y_t - y_i}{x_t - x_i}\right)$ to obtain the current look-angle $\epsilon_i = \gamma_i - \lambda_i$. The proposed controller modifies the look-angle of each pursuer and drives the trajectory of each pursuer towards its desired trajectory.

The proposed controller can mitigate heading errors using suitable controller gains K_1 and K_2. Then, the desired look-angles can be achieved, leading to nominal pursuers' trajectories derived which can be obtained from the geometrical rules. Additionally, we observed that constraints over the look-angles of the pursuers can also be handled by implementing this controller. As expected, heading errors and look-angle constraints can increase the impact time of the group beyond the specified impact time, yet simultaneous interception is still achieved due to the cooperative implementation of the geometrical rules using cyclic pursuit and leader follower protocols. Now, having derived the guidance laws, we will study them using simulations in the following section.

D. Simulations Results

The theoretical results obtained so far are exemplified in this section via numerical simulations. Three scenarios are examined for the minimum impact time guidance law, which is based on the geometrical rule depicted in Eq. Eq. (5). Initially, we investigate the ideal case where no heading errors are present and the look-angle is not constrained. Then, the ability to handle heading errors and look-angle constraints is examined.

The desired impact time guidance laws, which are based on the geometrical rules depicted in Eq. Eq. (8) for the n-to-one communication topology and in Eq. Eq. (9) for the one-to-one communication topology are examined via two scenarios for each guidance law. In the first scenario we examine the ideal scenario. Next, a scenario in which heading errors are present is considered. Comparison between the different communication topologies is also presented.
The following conditions hold throughout this section,

- The target is stationary and is located at the origin $(0, 0)$.
- In all the figures, the target position and the launch point of any pursuer are denoted by an asterisk and a square box, respectively.
- The maximum lateral acceleration of each pursuer is 100 $\left[\frac{m}{sec^2}\right]$.
- The controller gains are $K_1 = 800\left[\frac{m}{rad \cdot sec^2}\right]$ and $K_2 = 30\left[\frac{m}{rad \cdot sec^3}\right]$.

1. *Minimum impact time guidance law*

IDEAL SCENARIO In this part, we investigate the minimum impact time guidance law for an ideal scenario, implying that no heading errors are present and there are no look-angle constraints. We consider four pursuers launched from different positions and moving towards the target with different speeds as described in Table 1.

Pursuer	v [m/sec]	x_0 [m]	y_0 [m]	Heading Error [deg]
1	125	-7071	-7071	0
2	180	10000	9000	0
3	170	5000	-6000	0
4	150	-8000	0	0

Table 1: Initial conditions - minimum impact time, ideal scenario

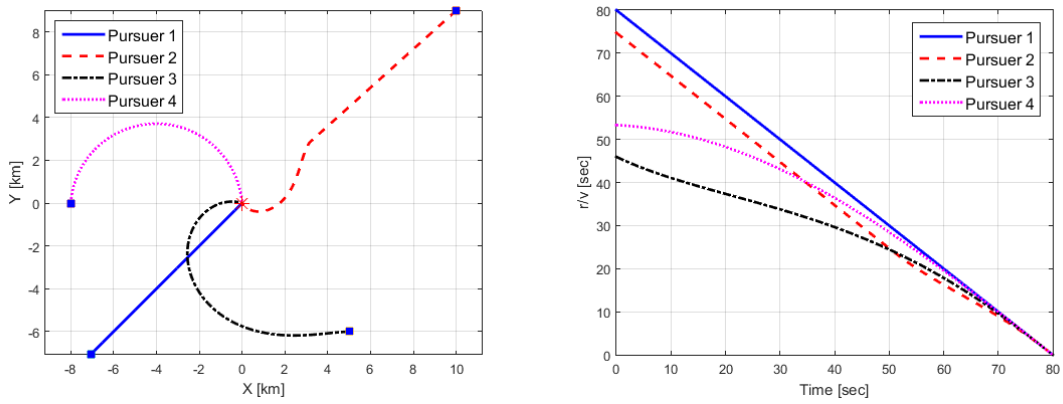

(a) Pursuers' trajectories

(b) Distance to speed ratio - $\tilde{t}$

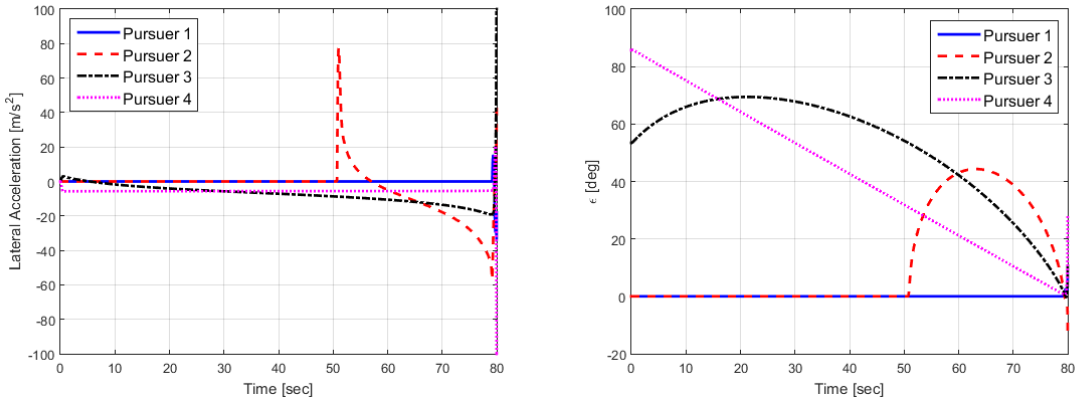

(c) Lateral acceleration

(d) Look-angles

Figure 7: Minimum impact time in an ideal scenario

The resulting trajectory, the parameter $\tilde{t} = \frac{r}{v}$, the look-angle, and the lateral acceleration are shown in Fig. 7. As illustrated from the figure, the pursuers reach the target simultaneously at $t = 80[sec]$. The initial conditions of the scenario dictate that $\tilde{t}_1(0) = \frac{r_1(0)}{v_1} = \max_{i\in\mathbb{N}_n}[\tilde{t}_i(0)] = 80[sec]$, which validates the claim in Theorem 1 that the common impact time is $\max_{i\in\mathbb{N}_n}[\tilde{t}_i(0)]$. It can also be seen in figure 7b that $\tilde{t}_1(t) = \max_{i\in\mathbb{N}_n}[\tilde{t}_i(t)]\ \forall t \in [0, 80]$, which also validates the theoretical results. Since $\tilde{t}_1(t) = \max_{i\in\mathbb{N}_n}[\tilde{t}_i(t)]\ \forall t \in [0, 80][sec]$, the trajectory of P_1 is a straight line, as depicted in Fig. 7a, and its look-angle throughout the engagement is equal to zero as shown in Fig. 7d. In Fig. 7c, we can see that since P_1 follows a trajectory of a straight line, its lateral acceleration is equal to zero throughout the engagement. Consequently, the trajectory of P_4, which receives information from P_1, is circular (Fig. 7a) as claimed in Corollary 1 and its look-angle profile is linear with respect to time (Fig. 7d). Additionally, the lateral acceleration of P_4 is constant, owing to its circular trajectory. Pursuer P_3 always changes its instantaneous circular trajectory as it receives information from P_4, which does not remain on a straight line, making its trajectory non-circular. The trajectory of P_2 is straight until $t = 51[sec]$, as its lateral acceleration and look-angle are zero (Fig. 7c and Fig. 7d respectively). From that time point, the lateral acceleration and the look-angle of P_2 cease to be zero. This behaviour can be explained by Fig. 7b, showing that $\tilde{t}_2 > \tilde{t}_3\ \forall t \in [0, 51][sec]$, which according to Eq. Eq. (5) leads to $\epsilon_2 = 0\ \forall t \in [0, 51][sec]$. From that time point until interception, we can see that $\tilde{t}_2 < \tilde{t}_3$, hence $\epsilon_2 = \text{Asinc}(\tilde{t}_2/\tilde{t}_3)$ in that time interval.

2. Heading errors scenario

We now examine the case where heading errors are present. The speeds and initial conditions of the pursuers are as described in Table 2. In contrast to the previous case, each pursuer is launched with a heading error. The results in Fig. 8 show that despite the large heading errors, the interception of the target occurs simultaneously. Nevertheless, due to the heading errors, the interception occurs at $t = 62.3[sec]$ and not at $\max_{i\in\mathbb{N}_n}[\tilde{t}_i(0)] = \tilde{t}_3(0) = \frac{r_3(0)}{v_3} = 60[sec]$. As seen in Fig. 8c, at the first 4 seconds of the engagement, the pursuers reach their lateral acceleration limiters since the initial heading errors leads to significant lateral acceleration requirements. By $t = 7[sec]$ the lateral acceleration for each pursuer becomes relatively steady. As seen in Fig. 8b, P_3 holds the maximum $\tilde{t}$ throughout the engagement, hence it tends to move in a straight line. Consequently, its lateral acceleration and look-angle tend to zero (Fig. 8c and 8d). Additionally, P_2 tends to move in a circular trajectory, with a linear look-angle profile and a constant lateral acceleration. The transient nature of the system lead to enlargement of the lateral acceleration at the last second of the engagement. In particular, the lateral acceleration of P_2 and P_3 did not remain constant. This phenomenon occurred for all scenarios and did not prevent the system from reaching simultaneous interception.

Pursuer	v [m/sec]	x_0 [m]	y_0 [m]	Heading Error [deg]
1	340	1000	0	-120
2	220	-8000	8000	70
3	100	0	6000	150

Table 2: Initial conditions - minimum impact time, heading errors scenario

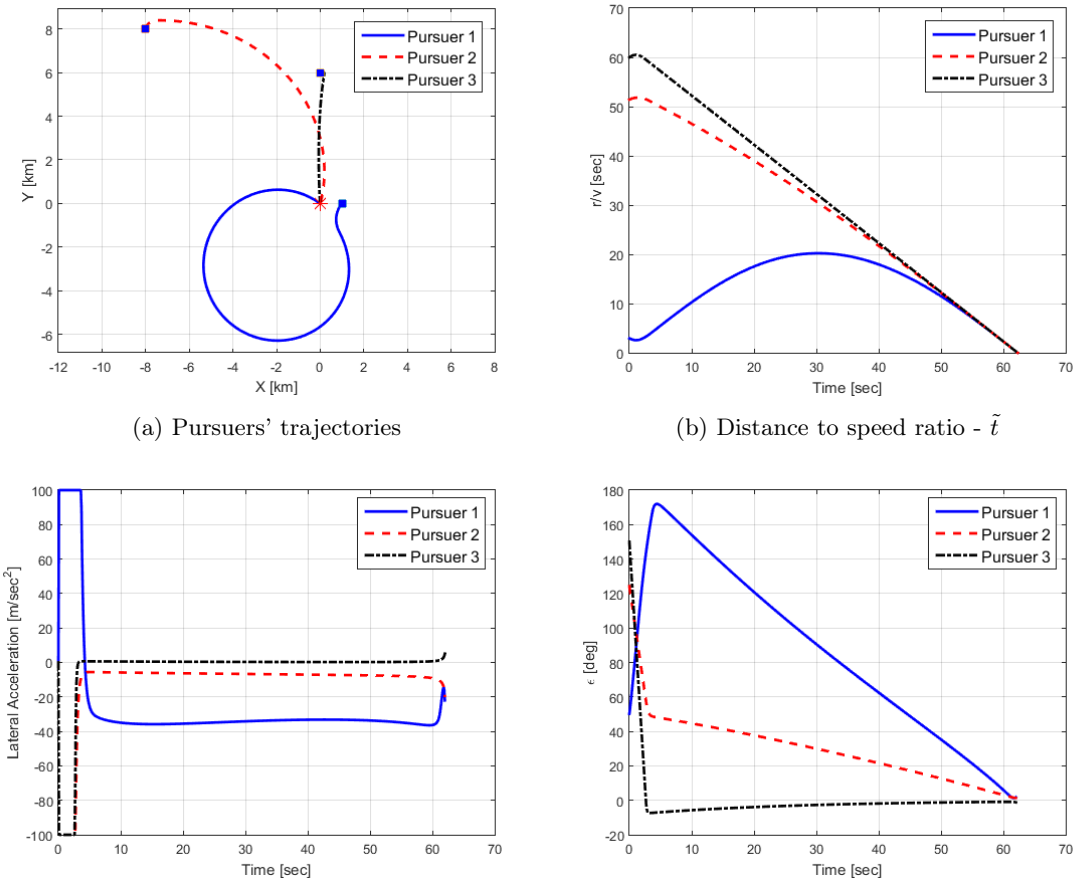

(a) Pursuers' trajectories

(b) Distance to speed ratio - $\tilde{t}$

(c) Lateral acceleration

(d) Look-angles

Figure 8: Minimum impact time law with heading errors

3. Heading errors and constrained look-angle scenario

Let us examine the case where in addition to having heading errors, the look-angle of the pursuers are also constrained. The speeds and initial conditions of the pursuers are as described in Table 3.

Pursuer	v [m/sec]	x_0 [m]	y_0 [m]	Heading Error [deg]
1	280	-7071	-7071	10
2	180	-7071	-6000	20
3	380	-7071	-5000	-40

Table 3: Initial conditions - minimum impact time, constrained look-angle scenario

Assume that the look-angle of each pursuer satisfies the constraint $|\epsilon| \leq \epsilon_{max}$, where $\epsilon_{max} = 80^o$. The results for this scenario are presented in Fig. 9. It can be noticed in Fig. 9b that in the initial seconds of the engagement, the look-angles of P_1 and P_3 are saturated at 80^o. Additionally, the lateral acceleration of P_3 reaches the limiters in the first 18 seconds (Fig. 9c). Simultaneous interception occurs despite the presence of heading errors and constrained look-angles, which shows the robustness of the guidance law.

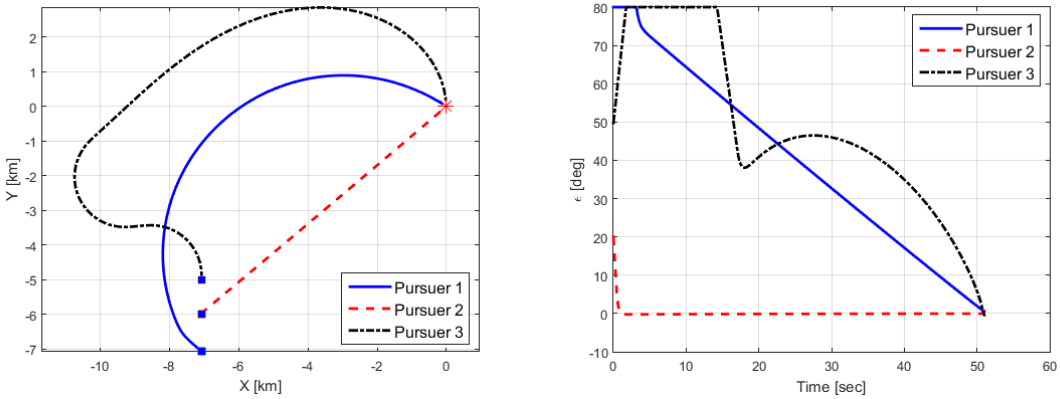

(a) Pursuers' trajectories

(b) Look-angles

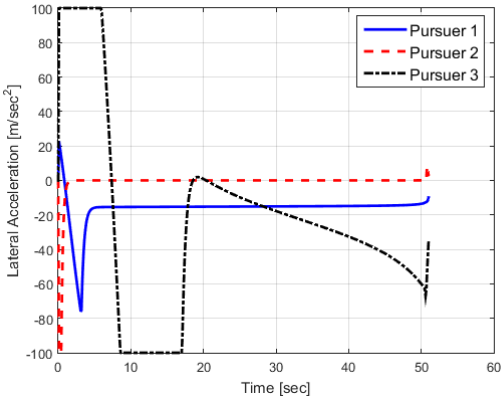

(c) Lateral acceleration

Figure 9: Minimum impact time law under constrained look-angle and heading errors

E. Desired impact time guidance law

1. *Ideal scenario*

In this part we will examine the implementation of the desired impact time geometrical rule in an ideal scenario. Two communication topologies are considered - the one-to-one and n-to-one topologies. No heading errors are present in this scenario. The speeds and initial conditions of the pursuers are as described in Table 4.

Pursuer	v [m/sec]	x_0 [m]	y_0 [m]	Heading Error [deg]
1	250	-7071	-7071	0
2	200	-7071	-7071	0
3	280	-7071	-7071	0
4	230	-7071	-7071	0

Table 4: Initial conditions - desired impact time, ideal scenario

The desired impact time is $t_d = 60[sec]$. Pursuer P_1 is the leader, which imposes the desired impact time guidance law independent of the rest of the pursuers in the system. In the one-to-one case, P_2 uses information from P_3, P_3 uses information from P_4 and, finally, P_4 uses information from the leader P_1. In the n-to-one case, P_2, P_3, and P_4 use information from the leader P_1 only. The results in Fig. 10 show that the pursuers achieve simultaneous interception in the desired impact time in both of the communication topologies. The trajectory of P_1 (Figs. 10a and 10b) is circular, as demonstrated by the linear look-angle profile in Figs. 10c and 10d. The trajectory of P_4 is identical in both cases since it refers to the leader P_1. The look-angle of P_2 is zero until $\tilde{t}_2$ becomes smaller than $\tilde{t}_3$, and a similar behaviour is viewed for P_4. Correspondingly, the lateral acceleration of P_2 and P_4, as depicted in Figs. 10e and 10f, are zero until their $\tilde{t}_i s$ become smaller than their respective $\tilde{t}_{i+1}$. The differences in the results between the two cases are not significant. Therefore, the choice between the two should be regarding the communication available, as explained in section 2.

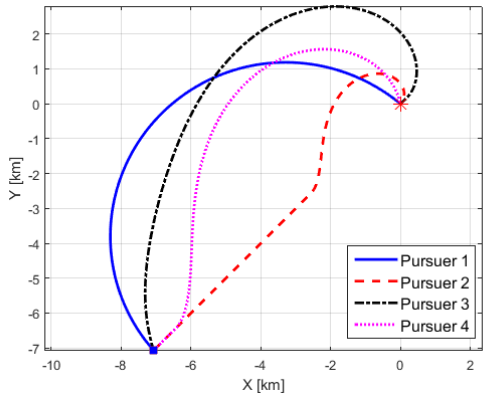

(a) Pursuers' trajectories, one-to-one

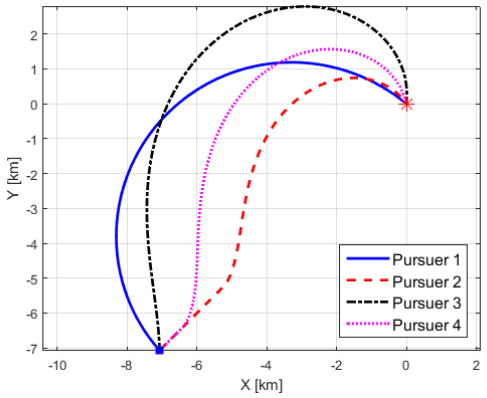

(b) Pursuers' trajectories, n-to-one

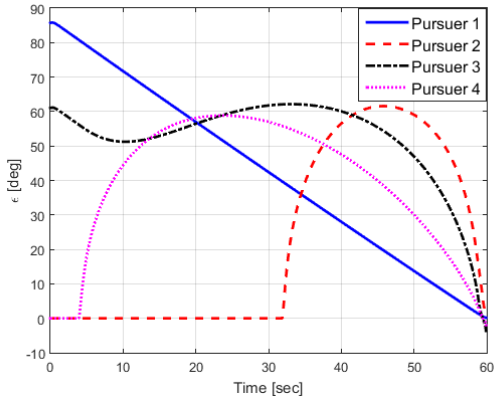

(c) Look-angles, one-to-one

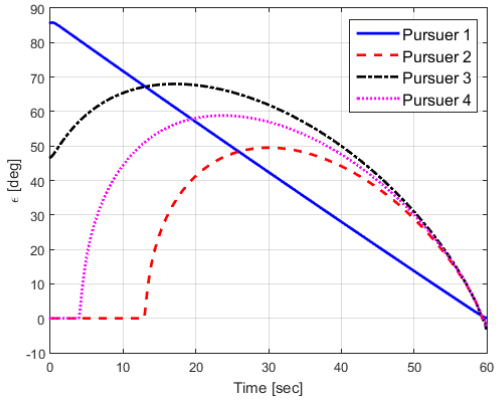

(d) Look-angles, n-to-one

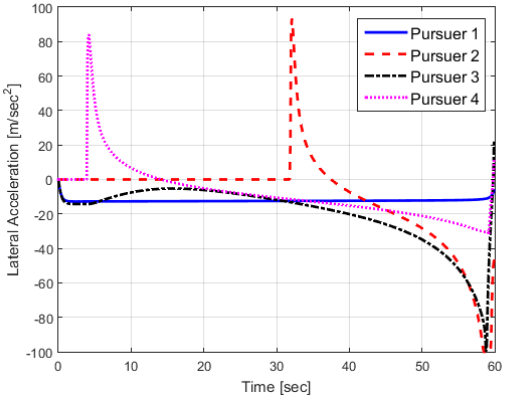

(e) Lateral acceleration, one-to-one

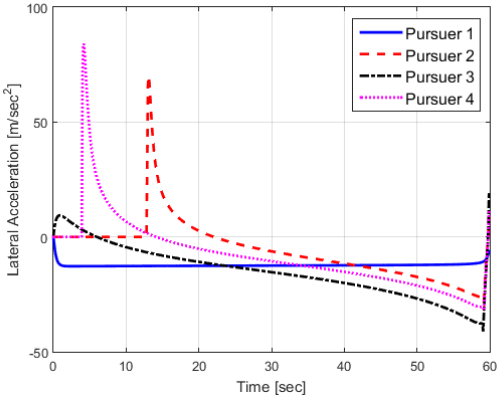

(f) Lateral acceleration, n-to-one

Figure 10: Desired impact time in an ideal scenario

HEADING ERRORS SCENARIO Now, we will examine the desired impact time guidance law in the presence of heading errors. The speeds and initial conditions of the pursuers are as described in Table 5.

Pursuer	v [m/sec]	x_0 [m]	y_0 [m]	Heading Error [deg]
1	300	-7071	-7071	20
2	180	0	11000	-40
3	220	8000	-4000	-120
4	240	-5000	0	45

Table 5: Initial conditions - desired impact time, heading errors scenario

The desired impact time is $t_d = 70[sec]$. The communication topologies are identical to the ones described for the ideal scenario. The results in Fig. 11 shows that simultaneous interception is achieved in the desired impact time despite the heading errors. By $t = 7[sec]$ the pursuers overcome their initial heading errors, as illustrated in the look-angle profiles in Figs. 11c and 11d. The lateral accelerations, depicted in Figs. 11e and 11f, show that it is slightly lower in the n-to-one communication topology than in the one-to-one case, especially at the the final seconds of the engagement.

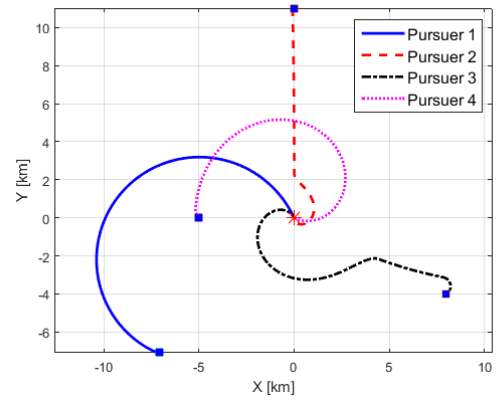

(a) Pursuers' trajectories, one-to-one

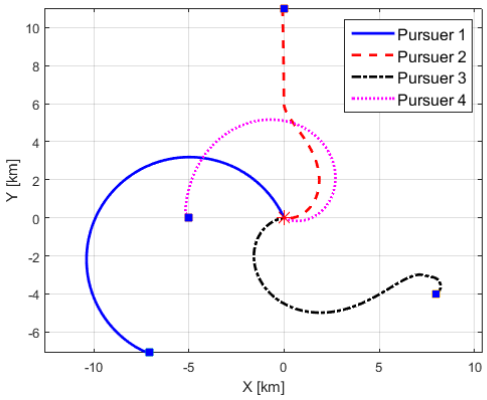

(b) Pursuers' trajectories, n-to-one

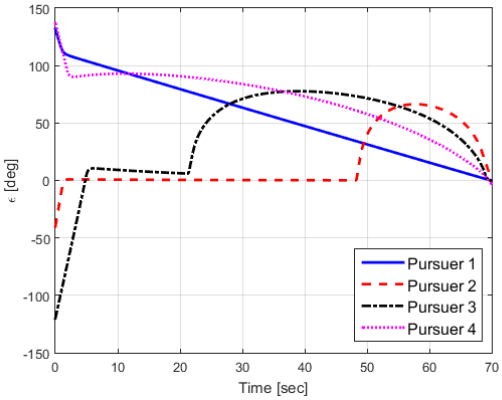

(c) Look-angles, one-to-one

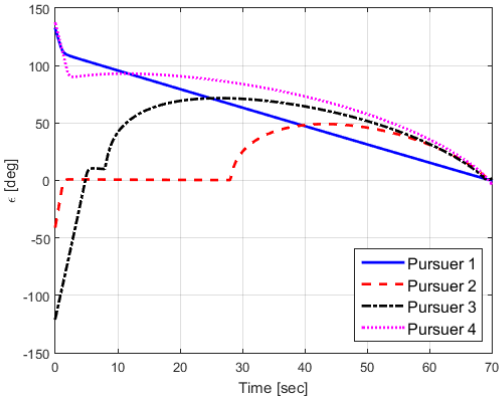

(d) Look-angles, n-to-one

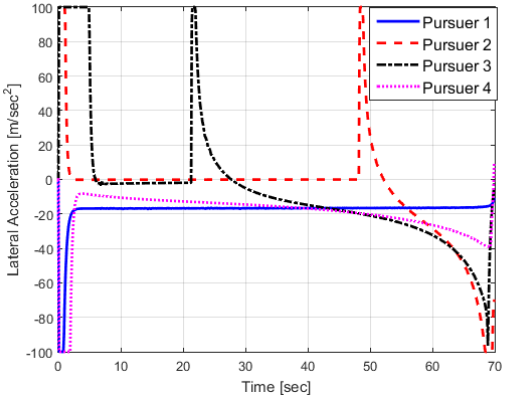

(e) Lateral acceleration, one-to-one

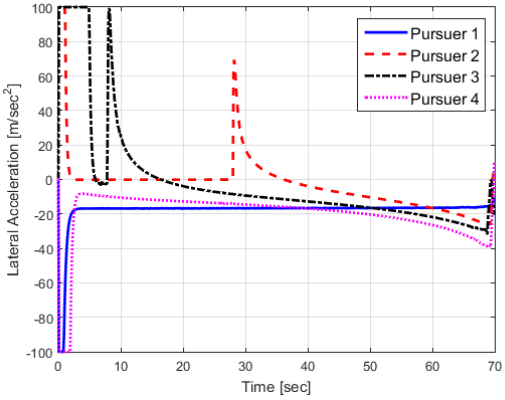

(f) Lateral acceleration, n-to-one

Figure 11: Desired impact time with heading errors

F. Results, discussions and conclusions

Cooperative guidance laws to achieve simultaneous target interception for a team of n pursuers were presented and investigated. Each pursuer adjusted its trajectory based on a geometrical rule governing its look-angle. To achieve simultaneous interception in the minimum possible time, a cyclic pursuit framework was applied, where each pursuer modified its trajectory with respect to its neighbour. For simultaneous interception in a desired impact time, the underlying geometrical rule was implemented using a leader-follower framework. The leader imposed the desired impact time and the followers modified their trajectory according to the leader. Two communication topologies were examined in the leader-follower framework. One of them is a one-to-one topology, where one follower communicated with the leader, whereas the rest of the followers communicated with their neighbours only. The second one is an n-to-one topology, where each follower modified its trajectory only according to the leader. For all of the geometrical rules, it was proved that simultaneous interception is guaranteed with arbitrary initial positions of the pursuers in the specified impact time. Simulation results showed that in the case where there were no heading errors or look-angle constraints, interception occurred at a time that was equal to the initial impact time of the pursuer that moved straight to the target, resulting in max-consensus in the ratio r_i/v_i as desired. The robustness of the guidance laws was shown by achieving simultaneous interception despite large heading errors and look-angle constraints. A comparison between the one-to-one and the n-to-one communication topologies showed minor differences, therefore choosing between the two should be based on the communication capabilities of the system. In the future, the case of a moving target would be considered. Additionally, different communication topologies, switching topologies, and time-delays can also be examined.

III. Minimum-Effort Impact-Time Control Guidance Using Quadratic Kinematics Approximation

A. Modeling and Problem Formulation

1. Nonlinear Kinematics

We consider a planar engagement between the missile M and the stationary target T. A schematic view is given in Fig. 12. The Cartesian frame Txy is attached to the target location and is aligned with the initial line-of-sight (LOS). The variable r stand foe range and λ denotes LOS angle. Missile speed, heading, and look angle are denoted as V, θ, and $\delta \triangleq \theta - \lambda$, respectively. Without the loss of generality, we assume $\lambda_0 = 0$, such that the initial heading and look angles are equal ($\theta_0 = \delta_0$). The missile is steered through the lateral acceleration a, applied perpendicular to the velocity vector.

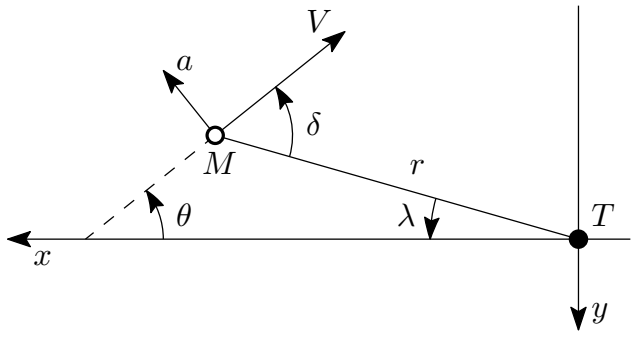

Figure 12: Planar engagement geometry.

We can express the nonlinear equations of motion (EOM) in the Cartesian frame as

$$\dot{x} = -V\cos\theta \tag{11}$$

$$\dot{y} = -V\sin\theta \tag{12}$$

$$\dot{\theta} = \frac{a}{V} \tag{13}$$

The kinematic EOM Eq. (11)–Eq. (12) can alternatively be written in the polar frame using range $r = \sqrt{x^2 + y^2}$ and LOS angle $\lambda = \arctan y/x$ as follows

$$\dot{r} = -V\cos\delta \tag{14}$$

$$\dot{\lambda} = -\frac{V}{r}\sin\delta \tag{15}$$

Henceforth for the guidance law derivation we assume: constant speed (V = const), ideal autopilot dynamics, i.e. $a(t)$ is a control signal, and $a(t)$ is unbounded.

2. Quadratic Kinematics (QK) Approximation

The kinematic equations are approximated using *second*-order Taylor series expansion of Eq. (11) and Eq. (12) around $\theta = 0$:

$$\dot{x} \simeq -V\left(1 - \frac{1}{2}\theta^2\right) \tag{16}$$

$$\dot{y} \simeq -V\theta \tag{17}$$

$$\dot{\theta} = \frac{a}{V} \tag{18}$$

where the equation Eq. (18) is left the same because it does not depend on the magnitude of θ. The system Eq. (16) – Eq. (18) is a complete set of EOM for the guidance law development. In contrast to conventional linearized EOM ($\dot{x} = -V$, $\dot{y} = -V\theta$, $\dot{\theta} = a/V$), where the final time has to satisfy $t_f = x_0/V$, the *quadratic* approximation allows *selecting* the desired t_f due to the quadratic term $\theta^2(t)$ in Eq. (16).

Remark 1. *The approximation Eq. (16)–Eq. (18) does not reduce the set of attainability (the set of states $\{x, y, \theta\}$ that can be reached whithin a given t_f) of the original system Eq. (11)–Eq. (13). Indeed, the equation for θ is unaffected by the approximation. Let $\boldsymbol{v} = [\dot{x}\ \dot{y}]^T$ be the velocity vector. Its magnitude for the original system Eq. (11)–Eq. (12) is always $||\boldsymbol{v}||_2 = V$. However, for the system Eq. (16)–Eq. (17) it is $||\boldsymbol{v}||_2 = V\sqrt{1+\theta^4/4} > V$ for all $\theta \in [-\pi, \pi]$. Thus, any target position that can be reached by the system Eq. (11)–Eq. (13), can be attained by Eq. (16)–Eq. (18) as well.*

B. Optimal Control Problem

We state the following minimum-effort nonlinear optimal control problem: minimize the quadratic cost

$$J = \frac{1}{2}\int_0^{t_f} a^2(t)\mathrm{d}t \tag{19}$$

subject to the EOM Eq. (16) – Eq. (18) with the boundary conditions

$$x_0 = r_0, \quad y_0 = 0, \quad \theta_0 = \text{fix} \tag{20}$$

$$x_f = 0, \quad y_f = 0, \quad \theta_f = \text{free} \tag{21}$$

given the fixed final time $t_f = \text{fix}$, satisfying $t_f > x_0/V$.

Remark 2. *For $x_0 = Vt_f$ and $\theta_0 = 0$ the trivial solution $a(t) = 0$, $t \in [0, t_f]$ is the trivial optimum which yields $J = 0$. If $x_0 = Vt_f$ and $\theta_0 \neq 0$, then there is no solution that can be implemented for the original nonlinear system. Hence, we assume $x_0 < Vt_f$ in the remainder of the work.*

Remark 3. *Because the optimization problem is posed with fixed terminal time, the results of the work may be directly extended to predictably moving targets. Then the stationary target T is simply replaced with the predicted intercept point (PIP).*

C. Optimal Control Solution

In this Section, we first state the main result of the work – the optimal solution to the problem exists for all permissible initial conditions and final time and there is a unique solution for $\theta_0 \neq 0$ and a pair of symmetric solutions for $\theta_0 = 0$. The result is proven in the remainder of the Section.

1. Statement of the Main Result

Let $u(\eta, \tau)$, $\eta \in \mathbb{R}$, $\tau \in [0, 1] \subset \mathbb{R}$ be the *shaping function* defined as

$$u(\eta, \tau) = \begin{cases} \dfrac{\sin \eta\tau}{\eta}, & \eta > 0 \\ \dfrac{\sinh \eta\tau}{\eta}, & \eta < 0 \\ \tau, & \eta = 0 \end{cases} \tag{22}$$

We denote its integral as $U(\eta, \tau) \triangleq \int_\tau^1 u(\eta, \tau)\,\mathrm{d}\tau$. The equation

$$D(\eta) = C_0 \tag{23}$$

is called the *discriminant equation*, in which $D(\eta)$ is the dimensionless *discriminant function*

$$D(\eta) \triangleq \frac{\left(\int_0^1 U(\eta, \tau)\,\mathrm{d}\tau\right)^2}{\int_0^1 U^2(\eta, \tau)\,\mathrm{d}\tau} \tag{24}$$

and $C_0 \in [0, 1)$ is the dimensionless *engagement parameter*

$$C_0 \triangleq \frac{\theta_0^2/2}{1 - x_0/(Vt_f) + \theta_0^2/2} \tag{25}$$

Finally, we define a binary sign function

$$s(\xi) = \begin{cases} 1, & \xi \geq 0 \\ -1, & \xi < 0 \end{cases} \tag{26}$$

With these notations, we state the main result of the work as follows

Theorem 1. There exists a unique optimal solution to the problem for $\theta_0 \neq 0$ and a pair of equal-cost symmetric solutions for $\theta_0 = 0$. The optimal solution is

$$a(t) = Ku\left(\eta, \tfrac{t_f - t}{t_f}\right), \quad t \in [0, t_f] \tag{27}$$

where η is the smallest solution of the discriminant equation, and

$$K = -s(\theta_0)\sqrt{\frac{2}{\int_0^1 U^2(\eta, \tau)}}\,\frac{V}{t_f}\,\sqrt{1 - \frac{x_0}{Vt_f} + \frac{\theta_0^2}{2}} \tag{28}$$

which for $\theta_0 = 0$ may be taken with the opposite sign.

2. *Proof of the Main Result*

The existence of the optimal solution may be straightforwardly asserted from [23, p. 88] once the problem is converted into Mayer form by introducing an additional state $\dot{\varphi}(t) = a^2(t)/2$, $\varphi(0) = 0$ and rewriting the cost as terminal: $J = \varphi(t_f)$.

We obtain the candidate solution using the Minimum Principle [24, Chapter 4] as follows.

Lemma 2. The candidate solutions to the problem are of the form

$$a(t) = Ku\left(\eta, \tfrac{t_f - t}{t_f}\right), \quad t \in [0, t_f] \tag{29}$$

where $K, \eta \in \mathbb{R}$ are constant parameters.

Proof. The Hamiltonian of the optimization problem is

$$H(\boldsymbol{x}, \boldsymbol{\psi}, a, t) = \frac{1}{2}\psi_0 a^2 - \psi_x V\left(1 - \frac{1}{2}\theta^2\right) - \psi_y V\theta + \psi_\theta \frac{a}{V} \tag{30}$$

where $\boldsymbol{x} = [x \;\; y \;\; \theta]^T$ is the state vector, $\boldsymbol{\psi} = [\psi_x \;\; \psi_y \;\; \psi_\theta]^T$ is the corresponding co-state vector and $\psi_0 \geq 0$ is a nonnegative scalar. The co-state equations and the transversality conditions are

$$\dot{\psi}_x(t) = -H'_x = 0, \quad \psi_x(t_f) = \text{free} \Rightarrow \psi_x = \text{const} \tag{31}$$

$$\dot{\psi}_y(t) = -H'_y = 0, \quad \psi_y(t_f) = \text{free} \Rightarrow \psi_y = \text{const} \tag{32}$$

$$\dot{\psi}_\theta(t) = -H'_\theta = \psi_y V - \psi_x V\theta(t), \quad \psi_\theta(t_f) = 0 \tag{33}$$

The system Eq. (16) – Eq. (18) is autonomous; hence, the Hamiltonian Eq. (30) is a constant of motion ($H = \text{const}$). The exact value of H is unspecified because the final time t_f is fixed. By the Minimum Principle, the optimal control $a(t)$ minimizes the Hamiltonian. Since the control is assumed unbounded we use the condition $H'_a = 0$ that leads to the equality $\psi_0 a = -\psi_\theta / V$. Analogously to [25] we demonstrate that $\psi_0 \neq 0$. Indeed, if $\psi_0 = 0$, then $\psi_\theta = 0$ and, consequently, $\dot{\psi}_\theta = 0$. But then, by the co-state equation Eq. (33), the angle $\theta(t)$, $t \in [0, t_f]$ must be constant; hence, $a(t) = 0$, $t \in [0, t_f]$. This will be the solution only in the case $x_0 = Vt_f$ and $\theta_0 = 0$, which by Remark 2 we do not consider. Since the minimum of the Hamiltonian may assume arbitrary value, the co-state vector may always be scaled to let $\psi_0 = 1$. Then, we obtain the expression for the candidate solution as:

$$a(t) = -\frac{\psi_\theta(t)}{V} \tag{34}$$

Because $\psi_\theta(t)$ is at least twice-differentiable, we take the time-derivative of Eq. (33), substitute $\psi_\theta(t) = -Va(t)$ from Eq. (34), and obtain the following second-order differential equation w.r.t. $a(t)$

$$\ddot{a}(t) - \frac{\psi_x}{V}a(t) = 0 \tag{35}$$

Equation Eq. (33) combined with Eq. (34) provides the boundary conditions as follows

$$a(t_f) = 0, \quad \dot{a}(0) = \psi_x \theta_0 - \psi_y = \text{const} \tag{36}$$

The class of real functions that describe the solution of Eq. (35) depends on the sign of ψ_x (negative, positive or zero). Define

$$\eta \triangleq -\text{sign}\,(\psi_x)\, t_f \sqrt{\frac{|\psi_x|}{V}} \tag{37}$$

Then the solution of Eq. (35) – Eq. (36) can be written as Eq. (29). □

Thus, the candidate solution is defined via the shaping function Eq. (22) illustrated in the Fig. 13. Because $a(t)$ is merely a scaling of the shaping function, the latter illustrates the behavior of the solution as a function of normalized time-to-go $\tau = \frac{t_f - t}{t_f}$.

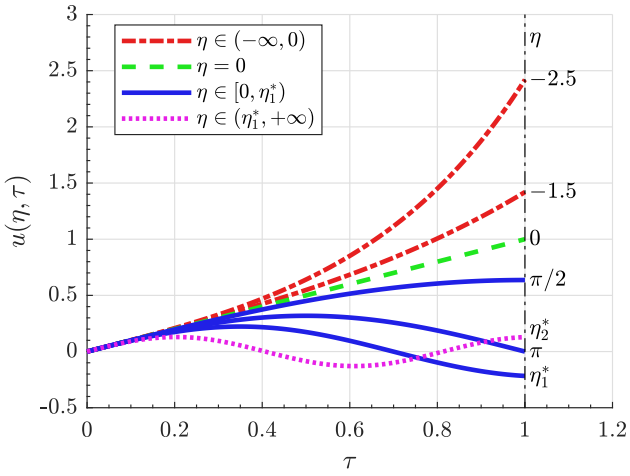

Figure 13: Shaping functions.

To determine the parameters K, η of the candidate solution Eq. (29), we substitute it into the EOM Eq. (16) – Eq. (18) and integrate from 0 to t_f, which results in the following system of equations w.r.t. K and η

$$K^2 \int_0^1 U^2(\eta, \tau)\, \mathrm{d}\tau = \frac{2V^2}{t_f^2}\left(1 - \frac{x_0}{V t_f} + \frac{\theta_0^2}{2}\right) \tag{38}$$

$$K \int_0^1 U(\eta, \tau)\, \mathrm{d}\tau = -\frac{V\theta_0}{t_f} \tag{39}$$

where

$$\int_0^1 U(\eta, \tau)\, \mathrm{d}\tau = \begin{cases} \frac{1}{\eta^3}\left(\sin\eta - \eta\cos\eta\right), & \eta > 0 \\ -\frac{1}{\eta^3}\left(\sinh\eta - \eta\cosh\eta\right), & \eta < 0 \\ 1/3, & \eta = 0 \end{cases} \tag{40}$$

$$\int_0^1 U^2(\eta, \tau)\, \mathrm{d}\tau = \begin{cases} \frac{1}{2\eta^6}\left(\eta^2 + 2\eta^2\cos^2\eta - 3\eta\sin\eta\cos\eta\right), & \eta > 0 \\ \frac{1}{2\eta^6}\left(\eta^2 + 2\eta^2\cosh^2\eta - 3\eta\sinh\eta\cosh\eta\right), & \eta < 0 \\ 2/15, & \eta = 0 \end{cases} \tag{41}$$

The full procedure of the EOM integration and the analytic expressions for the trajectories of Eq. (16) – Eq. (18) are given in Appendix B. Dividing Eq. (39) squared by Eq. (38) we discover that the parameter η of the candidate solution Eq. (29) satisfies the discriminant equation Eq. (23) with

$$D(\eta) = \begin{cases} \dfrac{2\left(\sin\eta - \eta\cos\eta\right)^2}{\eta^2 + 2\eta^2\cos^2\eta - 3\eta\sin\eta\cos\eta}, & \eta > 0 \\ \dfrac{2\left(\sinh\eta - \eta\cosh\eta\right)^2}{\eta^2 + 2\eta^2\cosh^2\eta - 3\eta\sinh\eta\cosh\eta}, & \eta < 0 \\ 5/6, & \eta = 0 \end{cases} \tag{42}$$

The discriminant equation possesses an important separation property – its left-hand part is a function of a single dimensionless control parameter η, and it is invariant w.r.t. the initial conditions and the final time. The initial conditions and t_f are all gathered in the right-hand part of the equation inside the dimensionless engagement parameter C_0. In Fig. 14 we present the plot of $D(\eta)$, using which the equation Eq. (23) can be interpreted graphically – the solutions are at the points of the intersections of $D(\eta)$ and a constant level C_0.

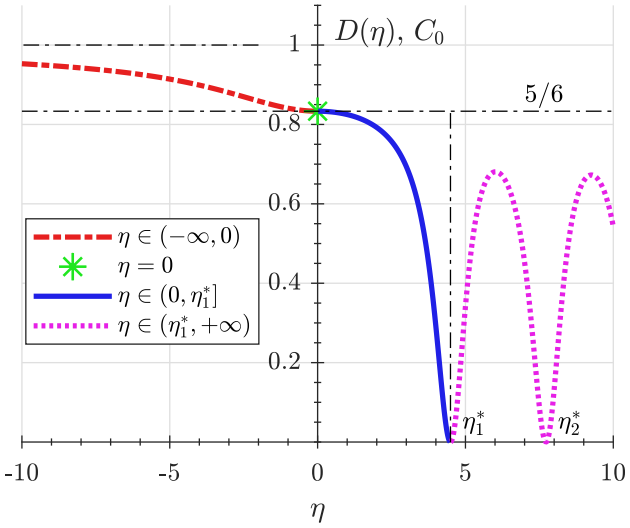

Figure 14: Graphical interpretation of eq. Eq. (23)

Let us define $\mathcal{S}(C_0) \triangleq \{\eta_i \,|\, D(\eta_i) = C_0, \eta_{i+1} > \eta_i, i = 1 \dots n \leq \infty\}$, to be the increasingly ordered solution set of the discriminant equation. We also introduce $\mathcal{S}^* \triangleq \{\eta_i^* \,|\, \eta_{i+1}^* > \eta_i^* > 0\, i = 1 \dots \infty\}$, as a set of increasingly ordered positive solutions of the equation $\sin\eta - \eta\cos\eta = 0$, namely $\eta_1^* \simeq 4.4934$, $\eta_2^* \simeq 7.7253$, $\eta_3^* \simeq 10.9041$, and so on. Then, we establish the following properties of the solution set.

Lemma 3. The discriminant equation has a unique nonpositive root $\eta \in \mathcal{S}(C_0) \leq 0$ if and only if $C_0 \in [5/6, 1)$.

Proof. By Lemma 8, the function $D(\eta)$, $\eta \leq 0$ is continuous, and it monotonically decreases from $\lim\limits_{\eta\to-\infty} D(\eta) = 1$ to $\lim\limits_{\eta\to 0} D(\eta) = 5/6$ on $\eta \in (-\infty, 0)$. Therefore, there is a unique nonpositive solution if $C_0 \in [5/6, 1)$. Conversely, if $\eta \leq 0$ then the image of $D(\eta)$ is $[5/6, 1)$. Hence, if $\eta \leq 0$ is a root of the discriminant equation, then $C_0 \in [5/6, 1)$. □

Lemma 4. The discriminant equation has a positive root $\eta \in \mathcal{S}(C_0) > 0$ if and only if $C_0 \in [0, 5/6)$. The smallest root $\eta \in (0, \eta_1^*]$ for all $C_0 \in [0, 5/6)$ yields the optimal value of the cost Eq. (19).

Proof. By Lemma 8, the function $D(\eta)$, $\eta > 0$ is continuous, and it monotonically decreases from $\lim\limits_{\eta\to 0} D(\eta) = 5/6$ to $D(\eta_1^*) = 0$ on $\eta \in (0, \eta_1^*)$. Then if $C_0 \in [0, 5/6)$, there always exists the smallest positive root on the interval $\eta \in (0, \eta_1^*]$. But by Lemma 9, the discriminant function is bounded as $D(\eta) < 5/6$ for $\eta > 0$; hence, the interval $[0, 5/6)$ is the image of $D(\eta)$ for positive η. Therefore, if $\eta > 0$ is a root then $C_0 \in [0, 5/6)$.

Substituting the candidate solution Eq. (29) into the cost Eq. (19), we obtain

$$J(K, \eta) = \frac{1}{2} K^2 t_f \int_0^1 u^2(\eta, \tau)\, \mathrm{d}\tau \tag{43}$$

where

$$\int_0^1 u^2(\eta, \tau) = \begin{cases} \frac{1}{2\eta^3}\left(\eta - \sin\eta\cos\eta\right), & \eta > 0 \\ -\frac{1}{2\eta^3}\left(\eta - \sinh\eta\cosh\eta\right), & \eta < 0 \\ 1/3, & \eta = 0 \end{cases} \tag{44}$$

According to Lemma 10, $\eta \in (0, \eta_1^*]$ yields smaller cost than any other $\eta \in \mathcal{S}(C_0)$. □

The auxiliary Lemmas used in the proofs above are given in the Appendix A. Combining the aforesaid Lemmas, the smallest root of the discriminant equation $\eta = \min \mathcal{S}(C_0)$ generates the optimal solution

Eq. (27). Using Eq. (38) we find K corresponding to η as in Eq. (28). Moreover, due to the continuity of $D(\eta)$, the root exists always for all permissible $C_0 \in [0, 1)$ and is unique because $D(\eta)$, $\eta \in (-\infty, \eta_1^*]$ is monotonically decreasing except for a single point. This completes the proof of the Theorem 1.

3. Control Effort and Maximal Maneuver

It is of great practical interest to evaluate such motion properties as missile control effort and maximal lateral acceleration during the engagement. Remarkably, for the proposed guidance law, they may be obtained semi-analytically given the initial conditions and the terminal time only as stated in the following theorems.

Theorem 5. The optimal control effort for the stated problem is

$$J = \frac{1}{G(C_0)} \frac{V^2}{t_f} \left(1 - \frac{x_0}{V t_f} + \frac{\theta_0^2}{2}\right) \tag{45}$$

where $G(C_0)$ is the inverse control effort coefficient defined as

$$G(C_0) = \frac{\int_0^1 U^2(\eta, \tau)\, \mathrm{d}\tau}{\int_0^1 u^2(\eta, \tau)\, \mathrm{d}\tau}, \quad \eta = \min \mathcal{S}(C_0) \tag{46}$$

Proof. Combining Eq. (43) and Eq. (28) we arrive at the stated result. □

Theorem 6. The maximal lateral acceleration along the optimal solution is

$$|a_m| = \frac{1}{M(C_0)} \frac{V}{t_f} \sqrt{1 - \frac{x_0}{V t_f} + \frac{\theta_0^2}{2}} \tag{47}$$

where $M(C_0)$ is a dimensionless coefficient defined as

$$M(C_0) \triangleq \begin{cases} \dfrac{\eta}{\sqrt{2} \sin \eta} \sqrt{\displaystyle\int_0^1 U^2(\eta, \tau)\, \mathrm{d}\tau}, & C_0 \in [8/\pi^2, 1) \\ \dfrac{\eta}{\sqrt{2}} \sqrt{\displaystyle\int_0^1 U^2(\eta, \tau)\, \mathrm{d}\tau}, & C_0 \in [0, 8/\pi^2) \end{cases} \tag{48}$$

and $\eta = \min \mathcal{S}(C_0)$.

Proof. Because $a = K u(\eta, \tau)$, where $K = \text{const}$, it is sufficient to find the maximal absolute value of $u(\eta, \tau)$ on $\tau \in [0, 1]$. For $\eta \le \pi/2$, the maximal value is at $\tau = 1$. For $\eta \in (\pi/2, \eta_1^*)$, there is a single extremum at $\tau^* = \frac{\pi}{2\eta}$, which is also the maximal absolute value. For $\eta = \eta_1^*$, there are two extremal points at $\tau_1^* = \frac{\pi}{2\eta_1^*}$ and $\tau_2^* = 1$, which are equal. Therefore, the maximal lateral acceleration may be computed as

$$|a(\tau)|_{\max} = |K| \times \begin{cases} u(\eta, 1), & \eta \le \pi/2 \\ 1/\eta, & \eta \in (\pi/2, \eta_1^*] \end{cases} \tag{49}$$

where the conditions on η may be replaced by $C_0 \in [8/\pi^2, 1)$ and $C_0 \in [0, 8/\pi^2)$ using Eq. (42), respectively. K may be taken as in Eq. (28). □

The control effort and maximal maneuver can be estimated by interpolation of the look-up tables $G(C_0) = \{G(\eta) \,|\, D(\eta) = C_0\}$ and $M(C_0) = \{M(\eta) \,|\, D(\eta) = C_0\}$ – these functions are depicted in the Fig. 15.

D. Closed-Loop Implementation

The optimal control solution Eq. (27) provides an open-loop command $a(t)$ depending on the initial conditions x_0, θ_0 and the final time t_f for the system Eq. (16)–Eq. (18). To implement it for the original nonlinear system Eq. (11)–Eq. (13), we propose re-initializing the solution of the optimal control problem at each time t, thus replacing t_f, x_0, and θ_0 with $t_{go} \triangleq t_f - t$, $r(t)$, and $\delta(t)$, respectively, and applying at each time instance the control $a(t) = K u(\eta, 1)$.

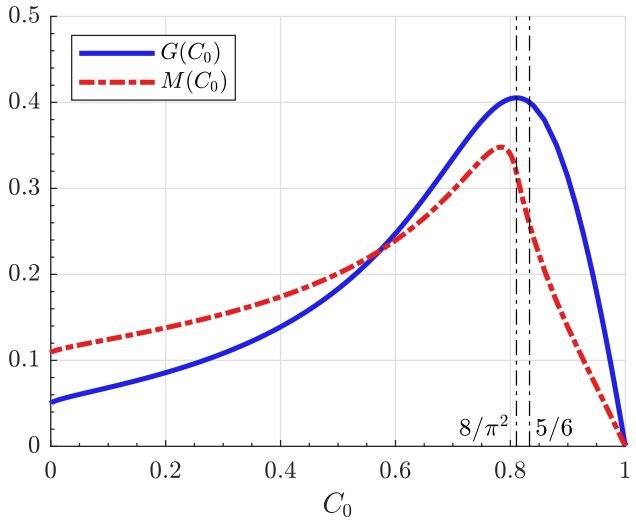

Figure 15: Table functions for evaluating control effort and maximal maneuver.

Remark 4. *The proposed implementation scheme realizes an approximation of the optimal solution. Recall that the solution of the optimization problem was derived for $y_0 = 0$. However, to rigorously implement the optimal control solution in closed-loop, it has to account for arbitrary y_0. But if y_0 is sufficiently small (hence, LOS angle λ is small too), then the implementation scheme above is a valid approximation. The reason to use it is that the optimal solution for the approximate problem now has to be implemented on a different system – the original nonlinear kinematics; therefore, the guidance law has to be expressed in terms of variables that are intrinsic to the guidance process – range, LOS rate, look angle, etc.*

1. Algorithmic Form of the Guidance Law

Using the procedure described above for the equations Eq. (27) and Eq. (28), we obtain the algorithmic form of the guidance law as follows

$$a(t) = -s(\delta) N_A(C) \frac{V}{t_{go}} \sqrt{1 - \frac{r}{V t_{go}} + \frac{\delta^2}{2}} \tag{50}$$

where $N_A(C)$ is the *navigational coefficient* defined as

$$N_A(C) \triangleq u(\eta, 1) \sqrt{\frac{2}{\int_0^1 U^2(\eta, \tau)\, \mathrm{d}\tau}}, \quad \eta = \min \mathcal{S}(C) \tag{51}$$

and the engagement parameter is computed as

$$C(t) = \frac{\delta^2/2}{1 - r/(V t_{go}) + \delta^2/2} \tag{52}$$

Note that it is not necessary solve the discriminant equation $D(\eta) = C$ online directly. Instead, by varying $\eta \in (-1/\varepsilon, \eta_1^*]$ where ε is a sufficiently small positive number, we construct a lookup table of n points $\left\{D\left(\eta^{(k)}\right), N_A\left(\eta^{(k)}\right)\right\}$, $k = 1 \ldots n$, which establishes a direct mapping between the engagement parameter C and the navigational coefficient N. Spline interpolation can be used to find values N outside of the table nodes.

The navigational coefficient $N_A(C)$ is illustrated in the Fig. 16. If $\delta = 0$, and therefore $C = 0$, the coefficient $N_A(C)$ simplifies into $N_A(5/6) = -2\eta_1^* \simeq -8.9868$. Also, it is easy to verify that $N_A(5/6) = \sqrt{15} \simeq 3.8730$. For $C < 2/3$, $N_A(C)$ is negative meaning that the guidance law actively deviates the missile from the LOS for small C. Conversely, for $2/3 < C < 1$ the navigational assumes high positive values and rises to infinity as $C \to 1$ meaning that the guidance law will actively converge the missile to the shortest path to the target. The corresponding guidance loop is shown in the Fig. 17.

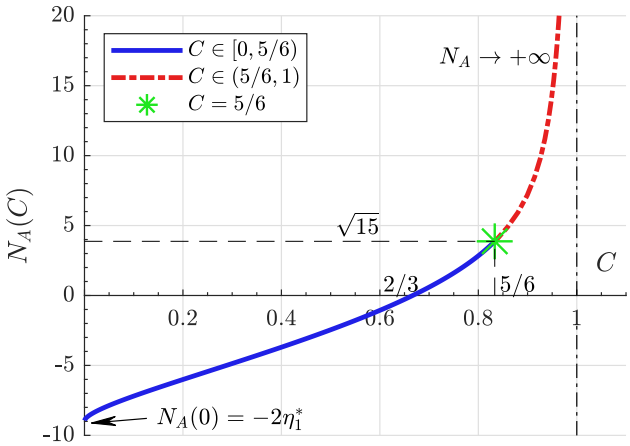

Figure 16: Navigational coefficient $N_A(C)$.

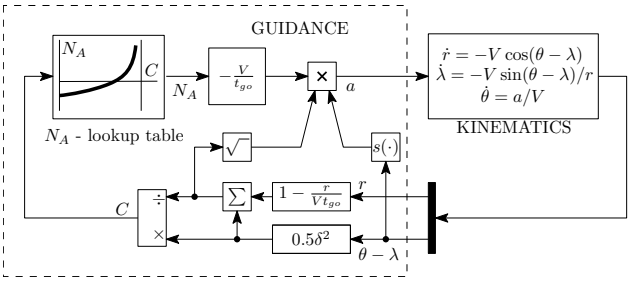

Figure 17: Guidance loop implementation according to eq. Eq. (50).

Thus, the guidance law implementation requires two measurements only: range r and look angle δ. The first may be obtained by an active radar, and the second one by any missile seeker.

2. *Implementation Using Passive-Only Information*

Now let us assume that only the measurements that can be obtained by a passive seeker, namely the look angle δ and the LOS rate $\dot{\lambda}$, are available. To develop the guidance law under this limitation, we alternatively use equations Eq. (27) and Eq. (39) instead of Eq. (38). Then performing the aforementioned state substitutions, the acceleration command assumes the following form

$$a(t) = -N_P(C)\frac{V\delta}{t_{go}}, \quad \delta \neq 0 \tag{53}$$

where

$$N_P(C) \triangleq \frac{u(\eta, 1)}{\int_0^1 U(\eta, \tau)\,\mathrm{d}\tau}, \quad \eta = \min \mathcal{S}(C) \setminus \mathcal{S}^* \tag{54}$$

To compute C we recall that $r = -V\sin\delta/\dot{\lambda}$ for $\delta, \dot{\lambda} \neq 0$ from Eq. (15) and obtain

$$C = \frac{\delta^2/2}{1 + \sin\delta/\left(\dot{\lambda}t_{go}\right) + \delta^2/2} \tag{55}$$

The function $N_P(C)$ is obtained analogously to the algorithmic form of the guidance law by constructing an interpolation table; its graph is shown in the Fig. 18. Unlike $N_A(C)$, $N_P(C)$ has an additional singularity at $C = 0$; thus, at $\delta_0 = 0$ the guidance law is undefined $(0 \cdot \infty)$. However, for practical purposes one may resort to open-loop control, e.g. a constant turn while C is small to escape the singularity of $N_P(C)$ and switch to the guidance law Eq. (53) when C exceeds the specified threshold. The gain $N_P(C)$ is negative

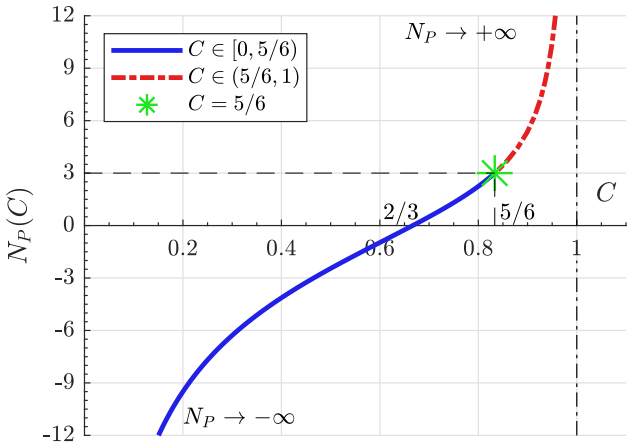

Figure 18: Navigational coefficient $N_P(C)$.

for $C < 2/3$, same as $N_A(C)$. Remarkably, $N_P(5/6) = 3$ – this allows us to establish the relation of the guidance law to proportional navigation (PN) in the following Lemma.

Lemma 7. Along the optimal trajectory, N_P converges to 3 as $t \to t_f$.

Proof. Recall the definition of η Eq. (37), in which η is proportional to t_f. Hence, in feedback implementation, $\eta(t)$ is proportional to t_{go}. Because $|\psi_x| < \infty$, we have $\lim_{t\to t_f} \eta(t) = 0$. Hence, $\lim_{t\to t_f} C(t) = 5/6$, which implies $\lim_{t\to t_f} N_P(t) = 3$. □

Also because $\lim_{t\to t_f} a(t) = 0$, the ratio between range r and closing speed $V_c = V\cos\delta$ converges to t_{go} determined by the running clock and the guidance law becomes $a(t) = 3V_c\dot{\lambda}$, which is PN with the gain of 3. Of course, because both the proposed implementations Eq. (50) and Eq. (53) realize the same solution Eq. (27), the guidance law shall converge to PN regardless of the implementation method. This has an important implementation consequence – switching to PN in the end of the engagement is a valid way to avoid the computational singularity of C at $t \to t_f$.

Furthermore, if throughout the engagement the angle δ is sufficiently small such that $-V\delta \simeq r\dot{\lambda}$ holds, the guidance law may be implemented in the following nonlinear PN-form

$$a(t) = N_P(C)\frac{t^a_{go}}{t^d_{go}}V_c\dot{\lambda} \tag{56}$$

where $V_c = V\cos\delta$ is the closing speed, $t^a_{go} = r/V_c$ is a first-order approximation of the time-to-go, and $t^d_{go} = t_f - t$ is the desired time-to-go determined by the running clock. There are two major differences from the classical PN ($3V_c\dot{\lambda}$). First, the navigational coefficient is a function of C, which, in the end, is a function of time. Second, the ratio r/V_c, except as $t \to t_f$, no longer approximates $t_{go} = t_f - t$, therefore, there is a corrective ratio t^a_{go}/t^d_{go} that compensates for this mismatch.

E. Numerical Simulation

In this Section, we present a series of numerical experiments to validate the developed guidance law performance. First, we present a study of the guidance law behavior in engagements with nonlinear kinematics. Second, we compare its performance effort to the four alternatives: impact-time control guidance [26], impact-angle selection scheme [27], adaptive impact-time control via the look-angle shaping [8], and numerically computed optimal nonlinear guidance. We furthermore, investigate the accuracy of the maximal acceleration prediction Eq. (47). Finally, we examine the influence of non-ideal flight dynamics on the guidance law performance.

Remark 5. *Throughout this Section, we shall study the set of engagements with the particular initial ranges and the missile speeds to present the results in a more intuitive fashion. However, because the studied problem is fixed-time, one can use the standard normalization:* $\bar{t} = t/t_f$, $\bar{x} = x/(Vt_f)$, $\bar{y} = y/(Vt_f)$, $\bar{a} = at_f/V$, $\bar{J} = t_f J/V^2$ *to transform the given results to the equivalent ones for different initial conditions, final time, and speed.*

1. Sample Trajectories

Consider a set of scenarios, in which $r_0 = 10$ [km], $\lambda_0 = 0$, $V = 500$ [m/s]. We remind that the target T is stationary. Ideal autopilot and sensors are assumed. Throughout this Section, we use the guidance law Eq. (50). The scenarios are as shown in the Table 6.

Table 6: Simulation scenarios.

# Scenario	θ_0 [deg]	t_f [s]
1	60	$21 \dots 30$
2	0	$21 \dots 35$
3	90	$50 \dots 300$

Scenario I. In this setting, we fix the launch angle at 60 [deg] and vary the final time in the range $t_f \in [21, 30]$ [s]. For comparison, the final time of the PN trajectory generated by the guidance command $3V_c\dot{\lambda}$ for the same launch angle is 22.41 [s]. To avoid the singularity in the computation of C, the guidance law switches to PN 0.5 [s] before impact. The simulation results for the quadratic kinematics (QK) guidance are presented in the Fig. 19.

The final times were chosen to demonstrate the guidance law behavior for the cases $\eta < 0$ ($t_f = 21$ [s]), $\eta \simeq 0$ ($t_f = 22.5$ [s]), and $\eta > 0$ ($t_f \in \{25, 30\}$ [s]). In all the cases we observe the expected behavior. For $t_f = 21$ [s], the acceleration command (Fig. 19b) starts at a high absolute value of 167 [m/s^2] (17 [g]) and exponentially decreases to 0 at the end. For the second engagement we chose the final time $t_f = 22.5$ [s] such that $C_0 \simeq 5/6$ – the engagement parameter stays close to this value throughout the flight (Fig. 19c), the acceleration profile is close to linear (Fig. 19b), and the navigational coefficient N_P is near 3 (Fig. 19d). Here and in the following simulations we obtained its value based on the simulation data using Eq. (53) as $N_P = -at_{go}/(V\delta)$. The other two scenarios ($t_f \in \{25, 30\}$ [s]) demonstrate the behavior, when the large final time forces the missile to leave its initial LOS and turn away from the target (see acceleration profiles, Fig. 19b, note the negative navigational coefficient near $t_{go} = 30$ [s] for the fourth case), and then approach it from a different direction.

The switch to the PN 0.5 [s] before the impact affected the impact-time negligibly - the errors did not exceed 10^{-6} [s]. The acceleration jump at the switch moment was smaller than 0.005 [m/s^2] for all cases, which evidently has a second-order small impact on the cost by the definition of J. The engagement parameter and the navigational coefficient were computed only for the time of QK-guidance law operation since the engagement parameter is meaningless in PN phase and is sensitive to the smallest changes of the states at the end. Implementing the guidance law using Eq. (53) and Eq. (55) yielded same results as presented above.

Scenario II. Here we examine the case, when the missile is launched at the target, but $r_0 < Vt_f$. We use the guidance law in the form Eq. (50). All the solutions in this case belong to the class $\eta > 0$. The acceleration profiles have two monotonicity regions and a change of sign, see Fig. 20b. Starting at $t_f = 30$ [s], we start to observe that the acceleration profile shape deviates from the theoretic sinusoidal form; however, the deformation is relatively small. This indicates that the second-order approximation assumptions hold even for look angles exceeding 90 [deg]. The engagement parameter C starts at 0 and increases to 5/6 as $t \to t_f$.

Scenario III. The purpose of this scenario is to demonstrate that the guidance law is able to handle large impact-time constraints and correct the impact-time errors, even when the derivation assumptions do not hold. We specify large required impact times $t_f \geq 50$ [s]. The simulation results are presented in the Fig. 21.

In all the considered cases, the time constraint was satisfied. However, we can no longer guarantee the optimality of the guidance law due to severe small look angle assumption violation: $\delta = \theta - \lambda$ was reaching 120-130 [deg]. The acceleration profiles in Fig. 21b may serve as an indication of this - they differ profoundly from the expected sinusoidal shape. But we note that as t_f increases, the trajectories tend to circles, which may be explained as follows. Recall that by our assumptions, we seeked a smooth control function Eq. (35). Moreover, Theorem 1 essentially constrains the number of monotonicity regions of the acceleration in the case $C_0 \in [0, 5/6)$. Therefore, an intuitive way to minimize the control effort is to apply the minimum "average" signal for most of the engagement time; hence, the tendency for circular trajectories for extremely

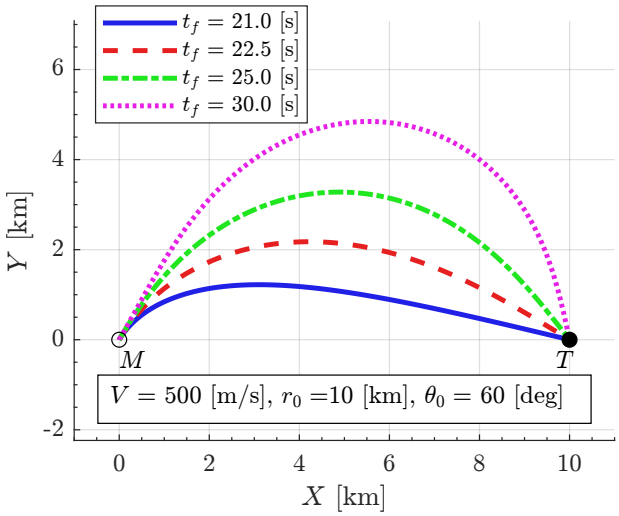

(a) Trajectories.

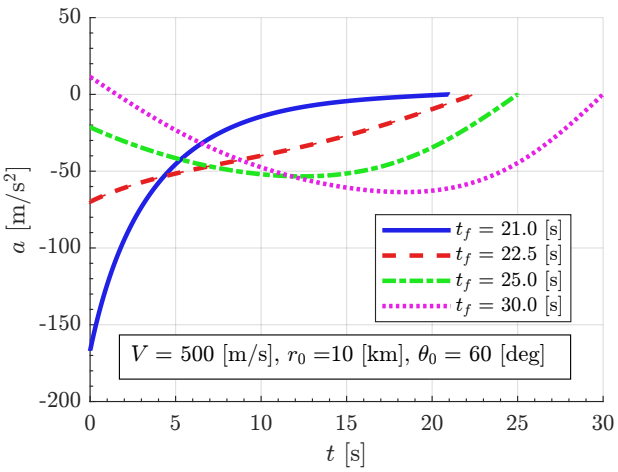

(b) Acceleration profiles.

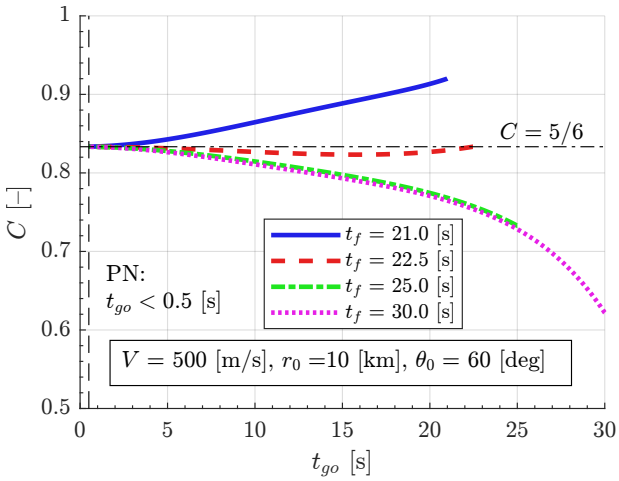

(c) Engagement parameter.

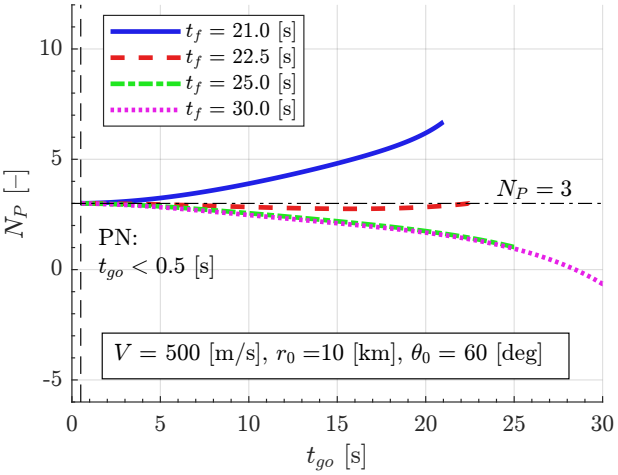

(d) Navigational coefficient.

Figure 19: Simulation results: Scenario I.

large t_f. Naturally, the navigational coefficient $N_P \simeq 2$ on near-circular path fragment [28, Chapter 5], see Fig. 21c.

2. *Analysis of Control Effort and Maximal Maneuver*

In the following simulation experiments, we shall compare the control-effort performance and the maximal lateral acceleration of the developed guidance law to the Refs. [26, 27, 8] and to the numerically obtained nonlinear optimal solution.

Consider a set of engagements with $r_0 = 10$ [km], $\theta_0 \in [30, 150]$ [deg] and the desired final time $t_f \in [21, 35]$ [sec]. For these engagements, we compare the control effort and maximal maneuver using the following four solution types for the *original nonlinear* EOM Eq. (11)–Eq. (13).

1. QK (actual) – QK guidance law Eq. (50) implemented in the feedback manner.
2. FALCON – numerically obtained optimal control solution using the FALCON optimization tool [29]. The nonlinear optimization problem consists of finding the minimum effort control $a(t)$ for a fixed terminal time problem s.t. the EOM Eq. (11)–Eq. (13).

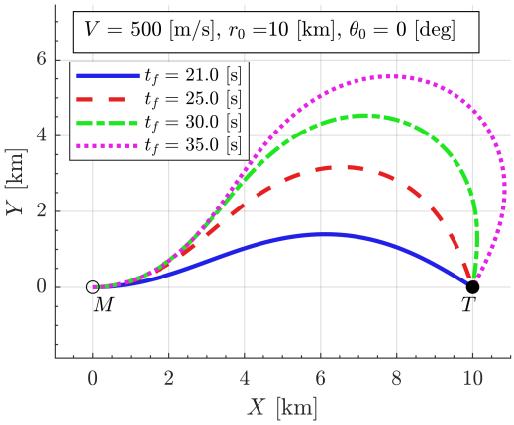

(a) Trajectories.

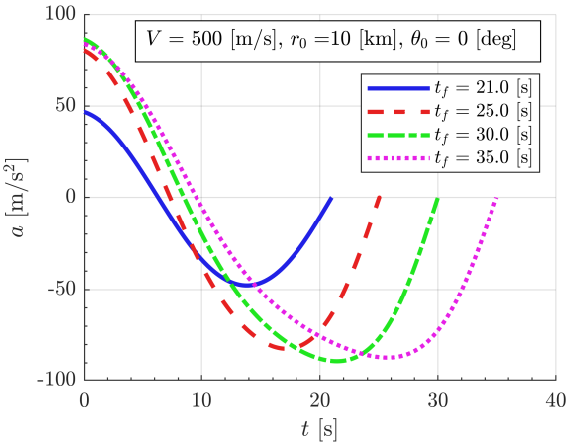

(b) Acceleration profiles.

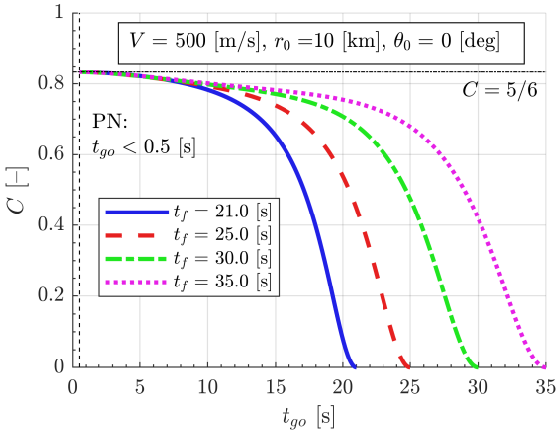

(c) Engagement parameter.

Figure 20: Simulation results: Scenario II.

3. ITCG – impact-time control guidance law [26], in which the acceleration command combines PN and time-correction terms. The latter is found using quadratic approximation of the path length. The implementation is $a = 3V\dot{\lambda} + K_\varepsilon \varepsilon_T$; $K_\varepsilon = -120V^5 / \left(3r^3 V\dot{\lambda}\right)$; $\varepsilon_T = (t_f - t) - \hat{t}_{go}$; $\hat{t}_{go} = \left(1 + 0.1\delta^2\right) r/V$.

4. ITC–θ_f – impact-time control via selecting the terminal impact angle. Ref. [27] provides the optimal solution to the impact-angle problem. However, the authors also develop practical time-to-go evaluation algorithms. To use the guidance law for the impact-time control, we fix the time-to-go t_{go} and find the terminal angle θ_f in closed-loop manner from the fourth-order polynomial given in Table 1, Method 2 in [27]. If multiple real solutions are present, the minimizer of the control effort (31) in [27] is selected. Having determined θ_f, the guidance law is implemented according to (26) in [27] as $a(t) = -V/t_{go} \cdot [6\delta + 2(\theta - \theta_f)]$.

5. AITC – adaptive impact-time control via look-angle shaping [8]. The guidance law (5) in [8]: $a(t) = V\left(\kappa(-t_{go})^n - n\delta/t_{go} + \dot{\lambda}\right)$ ($n = 2$ was used) was introduced based on look-angle shaping and quadratic approximation of the path length. The adaptation parameter κ is found in closed loop as one of the solutions of the second-order polynomial (20) in [8]: $\alpha_2\kappa^2 + \alpha_1\kappa + \alpha_0 = 0$, where $\alpha_2 = t_{go}^6/21$, $\alpha_1 = t_{go}\delta/3$, and $\alpha_0 = \delta^2 + 10\frac{r}{Vt_{go}}\left(\frac{r}{Vt_{go}^6} - 1\right)$.

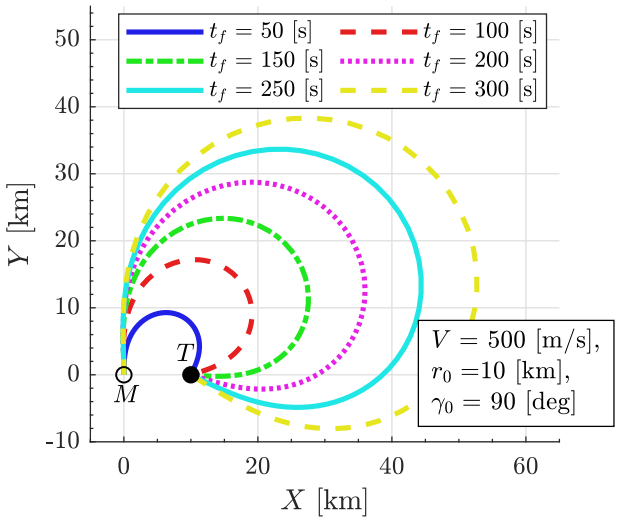

(a) Trajectories.

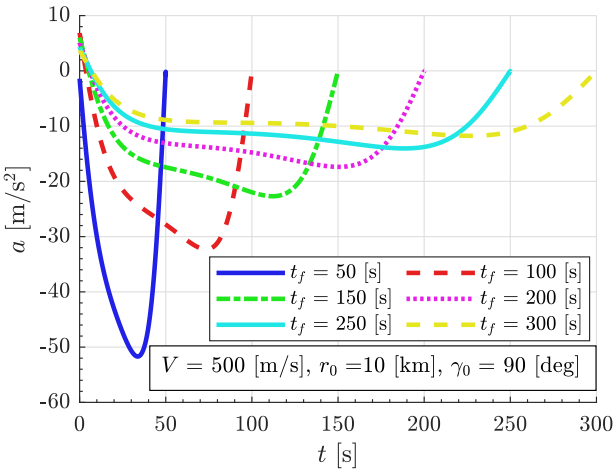

(b) Acceleration profiles.

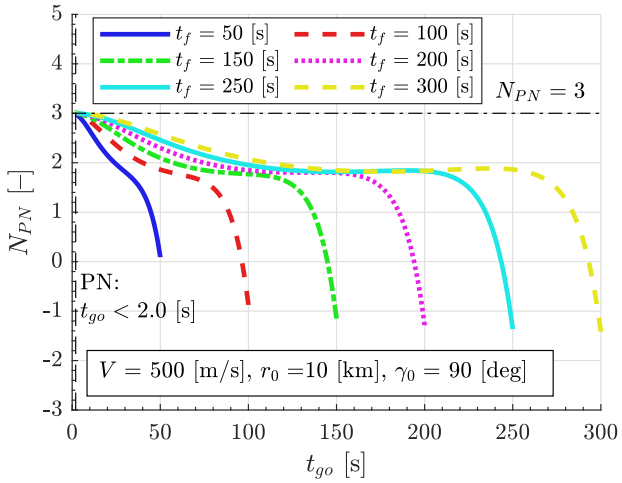

(c) Navigational coefficient.

Figure 21: Simulation results: Scenario III.

The simulation results for $\theta_0 = 30$ [deg] and $\theta_0 = 90$ [deg] are shown in the Fig. 22. All the considered guidance laws yield near-optimal control effort for small trajectory corrections. However, the performance of the proposed QK law is generally better for the larger final times and is consistent with the numerical optimal solution (we shall elaborate on it further). Although optimizing the control effort does not necessarily lead to maximal maneuver minimization, the maximal maneuver for QK is either similar for smaller final times or lower for the larger ones. Most importantly, the QK guidance law provides a feasible trajectory for all the considered initial conditions and final times – as expected from the optimal control solution existence. By contrast, the other guidance laws require the recursive solution of the polynomial equation, in which the existence of a real root for the feedback implementation is not guaranteed. Thus, for instance, the ITCG and AITC algorithms do not have solutions for $t_f < 23$ [s] and ITC–θ_f – for $t_f < 24$ [s] if $\theta_0 = 90$ [deg].

For the comparison convenience between the QK guidance and FALCON, we provide more detailed graphs in Fig. 23. Additionally to the feedback implementation of the proposed guidance law, we add the a-priori estimates (QK a-priori) using formulas Eq. (45) and Eq. (47). The plots in Fig. 23 (a-b) illustrate how the guidance effort and its a-priori estimate deviate from the optimal performance based on numerical optimization. In each plot, the right axis represents the actual control effort of the optimal solution, and the left axis represents the relative deviation ($\delta J = (J - J^*)/J^* \cdot 100\%$) of the proposed guidance law effort

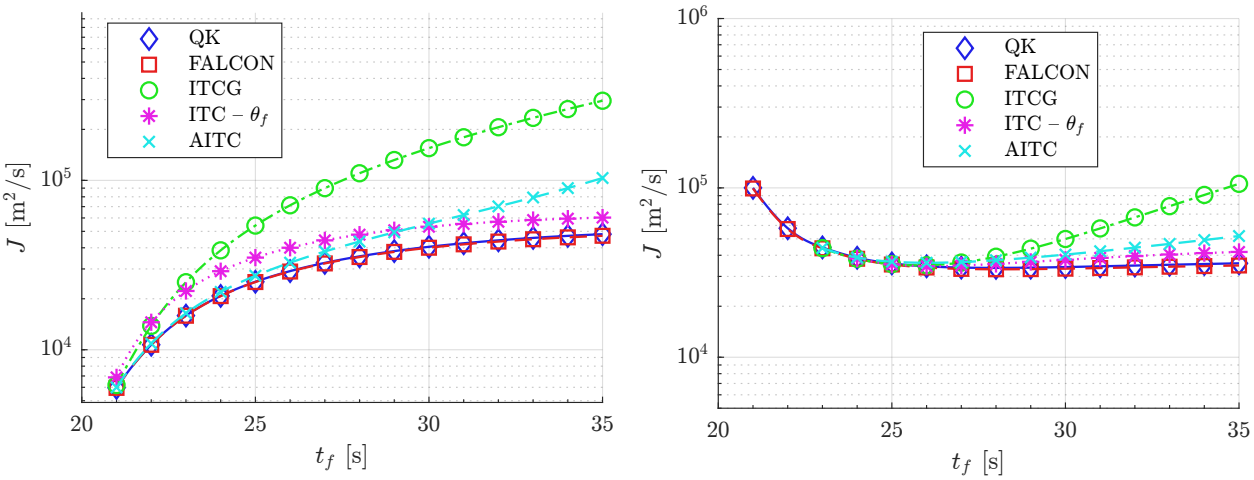

(a) Control effort, $\theta_0 = 30$ [deg].

(b) Control effort, $\theta_0 = 90$ [deg].

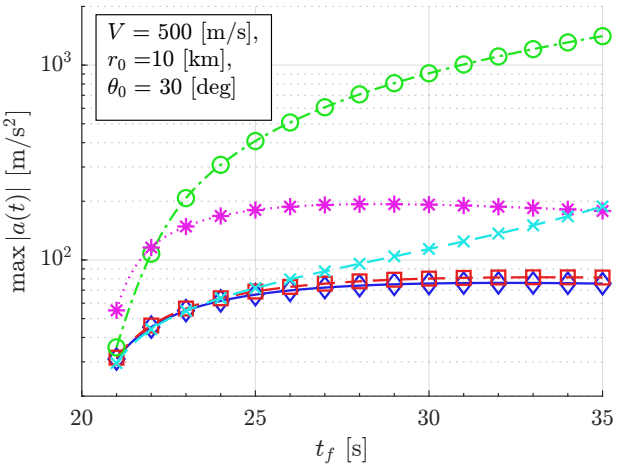

(c) Maximal maneuver, $\theta_0 = 30$ [deg].

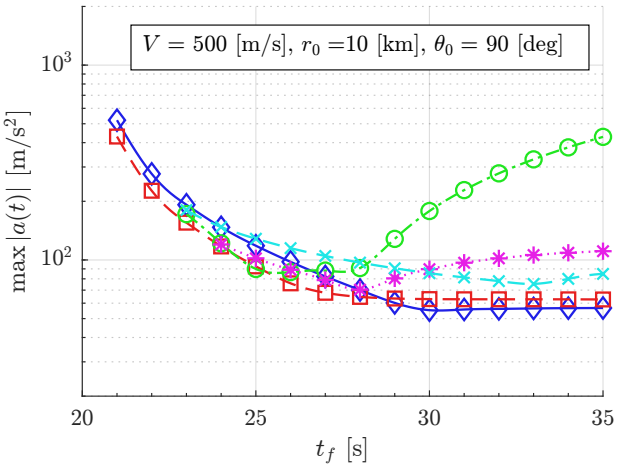

(d) Maximal maneuver, $\theta_0 = 90$ [deg].

Figure 22: Comparison of control effort and maximal maneuver.

J from the optimal solution J^*. A similar illustration is given in Fig. 23 (c-d) for the case of the maximal maneuver acceleration; the left axes show the difference between the QK and FALCON maximal maneuvers, i.e. $\Delta \max |a(t)| = \max |a(t)| - \max |a^*(t)|$.

In both the presented experiments, we observe that the QK solutions are close to the true optimal solution. The prediction of the cost using Eq. (45) may be slightly optimistic w.r.t. the actual result because it uses the approximate EOM for which the guidance law is truly optimal. For all the considered initial conditions and final times, the maximal relative cost deviation δJ of QK (actual) w.r.t. FALCON was not more than 10 %. The maximal relative cost prediction error using the open-loop solution was 12% for $\theta_0 < 90$ [deg] and 30% for $\theta_0 < 150$ [deg]. Thus, the QK guidance law yields a performance that is close to the optimal and can provide a reliable estimate of the required control effort based on the initial conditions and the final time only. The accuracy of open-loop calculation of the maximal required maneuver is significantly lower for large look angles, namely up to 80% for $\theta_0 = 150$ [deg]. However, for $\theta_0 \in \{30, 60, 90\}$ [deg], the relative errors w.r.t. FALCON solution are 6%, 12%, and 28%, respectively. Due to Remark 5, the provided dimensionless performance characteristics also hold for the different engagement settings.

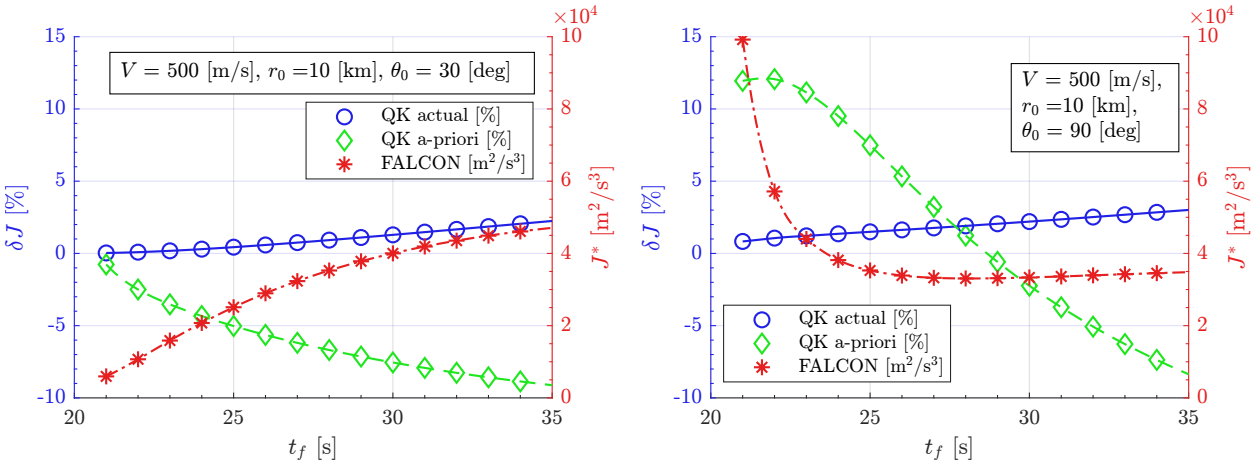

(a) Control effort, $\theta_0 = 30$ [deg].

(b) Control effort, $\theta_0 = 90$ [deg].

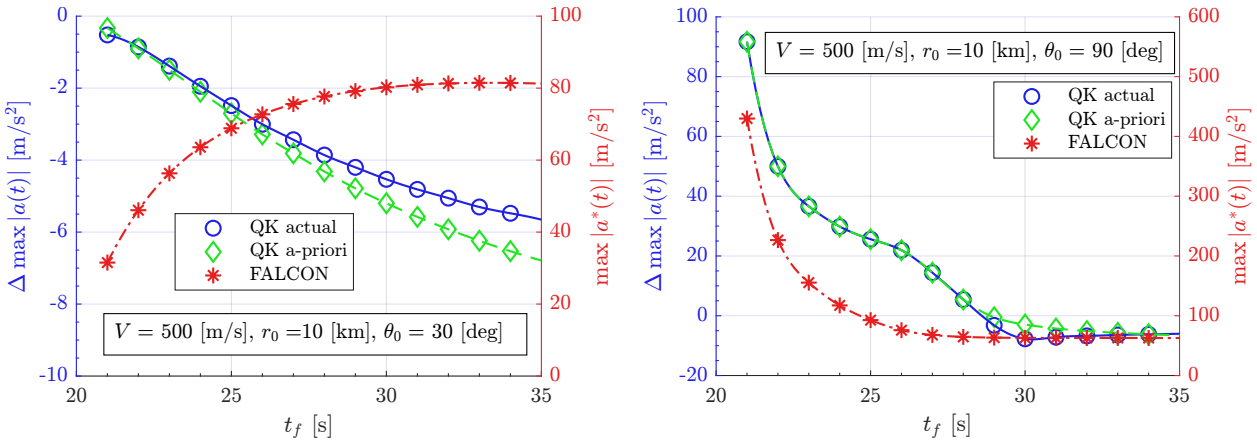

(c) Maximal maneuver, $\theta_0 = 30$ [deg].

(d) Maximal maneuver, $\theta_0 = 90$ [deg].

Figure 23: Comparison of control effort and maximal maneuver.

3. Autopilot Loop Dynamics Influence

Here, we shall provide the numerical examples of the autopilot loop dynamics influence on the guidance process. We consider linear first-order flight-control dynamics in the form $W_A(s) = 1/(Ts+1)$. Naturally, the larger the ratio T/t_f, the less is the influence of the autopilot dynamics on the guidance process. Therefore, to stress the autopilot impact, we scale down the example engagement to $r_0 = 5$ [km], $t_f = 11$ [s] leaving $V = 500$ [m/s] and $\theta_0 = 60$ [deg]. Fig. 24 shows the simulated trajectories and Fig. 25 – the corresponding guidance commands (thick lines) and the actual autopilot output (thin lines). The guidance law switches to OGL [28, 30, Chapters 8], which takes into an account the autopilot dynamics, 0.5 [s] before impact. Both the miss distance and the impact-time errors in the presented example were negligible ($< 10^{-5}$ [m] and $< 10^{-6}$ [s], respectively) for the realistic values of the time constants: $T \in [0.2, 0.4]$ [s]. A more thorough simulation study reveals that the similar performance holds as long as the switch to OGL is done $T \ldots 5T$ [s] before impact after approximately 2/3 of the engagement the trajectory was shaped by the QK guidance law.

F. Conclusions

The minimum-effort approach is employed to obtain the fixed-terminal time guidance law based on QK. Such a nonlinear optimal control problem is proven to generally have a unique solution, except in a symmetric case. The cost value and maximal maneuver formulas are derived semi-analytically in closed form.

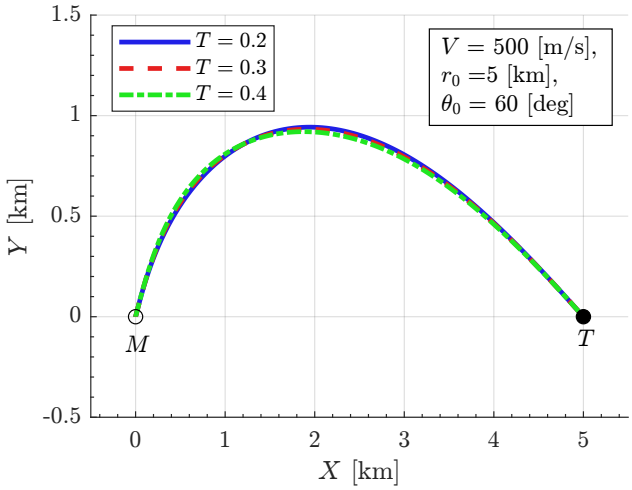

Figure 24: Trajectories of the missile with the first-order autopilot.

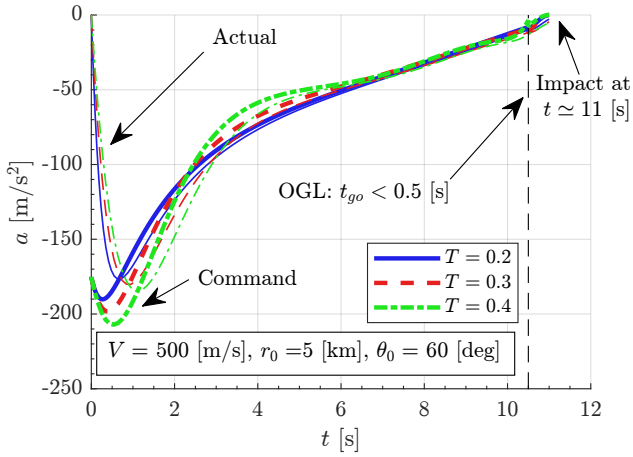

Figure 25: Lateral accelerations of the missile with the first-order autopilot.

Computationally efficient implementation procedures based on generally available sensor data are proposed. The simulation shows good agreement with the numerical optimization results. As anticipated, the proposed approach offers a two-fold improvement over the linearization-based methods. First, it principally allows specifying the final time of the trajectory, and second, it yields better results than existing sub-optimal solutions due to the direct optimization of the overall guidance command. However, remarkably, it also offers almost an analytic analysis framework, in contrast to the fully nonlinear problem. Thus, the proposed approach provides a convenient framework for designing the optimal guidance laws under a variety of constraints. Introducing additional impact angle or maneuver limitations can be the direction for future research.

Appendix

1. Auxiliary Lemmas

Lemma 8. The discriminant function $D(\eta) : \mathbb{R} \to [0, 1)$ is continuous for all $\eta \in \mathbb{R}$, surjective, and monotonically decreases on $\eta \in (-\infty, 0)$ and $\eta \in (0, \eta_1^*)$

Proof. Taking the limits one verifies $\lim_{\eta\to-0} D(\eta) = \lim_{\eta\to+0} D(\eta) = D(0) = 5/6$. In all other η, the discriminant function is continuous by definition; therefore, $D(\eta)$ is continuous for all $\eta \in \mathbb{R}$. Combining with $\lim_{\eta\to-\infty} D(\eta) = 1$, $D(\eta^*) = 0$, $\eta^* \in \mathcal{S}^*$, and the Cauchy-Schwarz inequality (strict for non-constant

functions)

$$\left(\int_0^1 U(\eta.\tau)\,\mathrm{d}\tau\right)^2 < \int_0^1 U^2(\eta,\tau)\,\mathrm{d}\tau \cdot \int_0^1 \mathrm{d}\tau \tag{A.1}$$

we establish the interval $[0,1)$ as the image of $D(\eta)$, so it is surjective w.r.t $[0,1)$.

Let us prove that $D(\eta)$, $\eta \in (0,\eta_1^*)$ is monotonically decreasing. Rewrite $D(\eta)$ for positive η as follows

$$D(\eta) = \frac{2f^2(\eta)}{g(\eta)}, \quad \eta > 0 \tag{A.2}$$

where $f(\eta) = \sin\eta - \eta\cos\eta$ and $g(\eta) = \eta^2 + 2\eta^2\cos^2\eta - 3\eta\sin\eta\cos\eta$. The derivative of $D(\eta)$ is

$$\frac{\mathrm{d}D(\eta)}{\mathrm{d}\eta} = -\frac{2f(\eta)}{g(\eta)}F(\eta), \quad \eta > 0 \tag{A.3}$$

where $F(\eta) = f(\eta)g'(\eta) - 2f'(\eta)g(\eta)$ is

$$F(\eta) \triangleq -\frac{3}{4}\cos\eta - 3\eta^2\cos\eta + \frac{3}{4}\cos 3\eta + \frac{21}{4}\eta\sin\eta - 2\eta^3\sin\eta + \frac{1}{4}\eta\sin 3\eta, \quad \eta > 0 \tag{A.4}$$

We claim that $F(\eta) > 0$ for $\eta \in (0, 5\pi/3)$, $5\pi/3 > \eta_1^*$. Indeed, It can be shown that $F(\eta)$ has the following Taylor series representation around $\eta = 0$

$$F(\eta) = \sum_{k=4}^{\infty}(-1)^k\,\frac{21(1-9^k) + 2k\left(1 + 3^{2k+1} + 8k(3+4k)\right)}{4(2k+2)!}\,\eta^{2k+2} \tag{A.5}$$

We verify that the alternating series coefficients are positive for $\forall k \geq 4$. Furthermore, the obtained series is absolutely convergent for $|\eta| < \infty$ because of the factorial in the denominator. Let F_n denote the n-th partial sum of Eq. (A.5). Then from the Leibniz test for sign-alternating series, the partial sum error and its sign are determined by the first neglected term [31]. Therefore, $F_n(\eta)$ for odd n will represent a lower bound on $F(\eta)$. Consider $F_{17}(\eta)$ – a polynomial of 36th degree with 10 zero roots. We find the first positive root to be approximately $5.58 > 5\pi/3 \simeq 5.24$. Therefore $F(\eta) > F_{17}(\eta) > 0$ for $\eta < 5\pi/3$. Therefore, because $-2f/g^2 < 0$ for $\eta \in (0,\eta_1^*)$ and $F(\eta) > 0$, $D'(\eta) < 0$ on $\eta \in (0,\eta_1^*)$.

Finally, let us prove that $D(\eta)$, $\eta \in (-\infty, 0)$ is monotonically decreasing as well. For short let us rewrite $D(\eta)$ for $\eta < 0$ as

$$D(\eta) = \frac{v(\eta)}{w(\eta)} \tag{A.6}$$

where $v(\eta) = \frac{1}{\eta^6}\left(\sin\eta - \eta\cos\eta\right)^2$ and $w(\eta) = \frac{1}{2\eta^6}\left(\eta^2 + 2\eta^2\cos^2\eta - 3\eta\sin\eta\cos\eta\right)$. Their series representations around $\eta = 0$ are

$$v(\eta) = 2^5\sum_{k=0}^{\infty}\frac{2k^2+7k+5}{2(2k+6)!}(2\eta)^{2k} \tag{A.7}$$

$$w(\eta) = 2^5\sum_{k=0}^{\infty}\frac{k^2+4k+3}{(2k+6)!}(2\eta)^{2k} \tag{A.8}$$

The series coefficients in Eq. (A.8) are positive $\forall k \geq 0$. Let us show that the sequence of the ratios of the coefficients $\{\Delta_k = 0.5(2k^2+7k+5)/(k^2+4k+3)\}$ is increasing. To that end, let us define an auxiliary function

$$\delta(\xi) = \frac{1}{2}\frac{2\xi^2+7\xi+5}{\xi^2+4\xi+1} \tag{A.9}$$

for which holds $\delta(k) = \Delta_k$. Taking the derivative w.r.t. ξ we obtain

$$\frac{d\delta(\xi)}{d\xi} = \frac{1}{2}\,\frac{1}{(\xi+3)^2} > 0, \quad \forall\xi \geq 0 \tag{A.10}$$

Then, by Lemma 1 from [32] the even quotient $v(\eta)/w(\eta)$ is monotonically increasing for $\eta > 0$; hence, the function $D(\eta)$ is monotonically decreasing on $\eta \in (-\infty, 0)$.

□

Lemma 9. The discriminant function $D(\eta) < 5/6$ for all $\eta > 0$.

Proof. Throughout this proof we shall assume that $\eta \notin \mathcal{S}^* \cup \{\pi/2 + \pi k \mid k \in \mathbb{Z}\}$ unless specified otherwise. Consider the expression of the cost Eq. (43). For $\theta_0 \neq 0$ we determine K using Eq. (39) and rewrite the cost Eq. (43) in the following form

$$J = \tilde{G}^{-1}(\eta)\,\frac{V^2}{t_f}\,\theta_0^2, \quad \theta_0 \neq 0 \tag{A.11}$$

where $\tilde{G}(\eta)$ is a a dimensionless coefficient defined as

$$\tilde{G}(\eta) \triangleq \frac{2\left(\int_0^1 U(\eta,\tau)\,\mathrm{d}\tau\right)^2}{\int_0^1 u^2(\eta,\tau)\,\mathrm{d}\tau} \tag{A.12}$$

Let us rewrite the discriminant equation and the control effort coefficient for $\eta > 0$ using $\tan\eta$ (divide both numerators and denominators by $\cos^2\eta$ and use $1/\cos^2\eta = 1 + \tan^2\eta$)

$$D^{-1}(\eta) = \frac{1}{2}\cdot\frac{\eta^2\tan^2\eta + 3\eta^2 - 3\eta\tan\eta}{(\tan\eta - \eta)^2} = C_0^{-1}, \quad \eta \in \mathcal{S}(C_0) \tag{A.13}$$

$$\tilde{G}^{-1}(\eta) = \frac{\eta^2}{4}\cdot\frac{\eta^2\tan^2\eta + \eta^2 - \eta\tan\eta}{(\tan\eta - \eta)^2} \tag{A.14}$$

from where we express $\tan\eta$ as

$$\tan\eta = \eta + \frac{\eta^3}{2\tilde{G}(\eta) - \eta^2 C_0^{-1}}, \quad \eta \in \mathcal{S}(C_0) \tag{A.15}$$

Substituting the obtained expression back into $D^{-1}(\eta) = C_0^{-1}$ results in the elimination of $\tan\eta$ and yields the following quadratic algebraic equation w.r.t. $\tilde{G}(\eta)$ at $\eta \in \mathcal{S}(C_0)$

$$4\tilde{G}^{-2}(\eta) - 2\left[2(C_0^{-1} - 1)\eta^2 + 3\right]\tilde{G}^{-1}(\eta) + (C_0^{-1} - 1)^2\eta^4 + \eta^2 C_0^{-1} = 0, \quad \eta \in \mathcal{S}(C_0) \tag{A.16}$$

Therefore, if the equation $D(\eta) = C_0$, $C_0 \in (0,1)$ has a solution for positive η, then it has a corresponding cost defined by $\tilde{G}(\eta)$ satisfying the above. Let us compute the discriminant of the equation Eq. (A.16) to find the values of C_0 for which the $\tilde{G}(\eta)$ may be determined

$$\mathcal{D} = 4(2C_0^{-1} - 3)\eta^2 + 9 \geq 0, \quad \eta \in \mathcal{S}(C_0) \tag{A.17}$$

hence, C_0^{-1} must satisfy

$$C_0^{-1} \geq \frac{3}{2} - \frac{9}{4\eta^2}, \quad \eta \in \mathcal{S}(C_0) \tag{A.18}$$

From where it follows that for $\eta > 4 < \eta_1^*$, $C_0 < 64/87 < 5/6$. Due to the equality $D(\eta) = C_0$, we extrapolate the result on $D(\eta)$. Note that it is not affected by the restraint assumed in the beginning of the proof, for the obtained expression is the upper bound; thus, $D(\eta_i^*) = 0 < 5/6$ is satisfied automatically. At the tangent singularities the result holds due to the continuity of $D(\eta)$. □

Lemma 10. For $C_0 \in [0, 5/6)$ the first root $\eta_1 \in \mathcal{S}(C_0) > 0$ provides the lowest cost functional value Eq. (43).

Proof. The idea of this proof is based on establishing a relation between the cost and the control parameter in a special form, from which it is easy to show that the cost is minimal if $\eta \leq \eta_1^*$. Throughout this proof we assume $\eta > 0$ by default. Let is return to the original system of equations Eq. (38)–Eq. (39). Squaring the second equation and taking the difference we obtain

$$K^2\left[\int_0^1 U^2(\eta,\tau)\,\mathrm{d}\tau - \left(\int_0^1 U(\eta,\tau)\,\mathrm{d}\tau\right)^2\right] = \frac{2V^2}{t_f^2}\left(1 - \frac{x_0}{Vt_f}\right) \tag{A.19}$$

For arbitrary η define

$$\hat{K}^2(\eta) \triangleq \frac{\frac{2V^2}{t_f^2}\left(1 - \frac{x_0}{Vt_f}\right)}{\int_0^1 U^2(\eta,\tau)\,\mathrm{d}\tau - \left(\int_0^1 U(\eta,\tau)\,\mathrm{d}\tau\right)^2} \tag{A.20}$$

for which holds $\hat{K}^2(\eta) = K^2$ if $\eta \in \mathcal{S}(C_0)$. Then using Eq. (43), we can calculate the cost based on the new expression for K:

$$J = \frac{1}{\hat{G}(\eta)} \frac{V^2}{t_f} \left(1 - \frac{x_0}{V t_f}\right), \quad \eta \in \mathcal{S}(C_0) \tag{A.21}$$

where $\hat{G}^{-1}(\eta)$ is a dimensionless coefficient computed as

$$\hat{G}(\eta) = \frac{\left(\int_0^1 U^2(\eta,\tau)\,\mathrm{d}\tau - \left(\int_0^1 U(\eta,\tau)\,\mathrm{d}\tau\right)^2\right)}{\int_0^1 u^2(\eta,\tau)\,\mathrm{d}\tau} \tag{A.22}$$

This function has no singularities for every $\eta \in \mathbb{R}$ and it does not depend on the boundary conditions of a particular engagement. For positive η, $\hat{G}(\eta)$ may be represented as

$$\hat{G}(\eta) = \frac{1}{\eta^2}\left(1 + \frac{2}{\eta} \cdot \frac{\eta \sin\eta\cos\eta - \sin^2\eta}{\eta - \sin\eta\cos\eta}\right), \quad \eta > 0 \tag{A.23}$$

and its plot is shown in the Fig. 26.

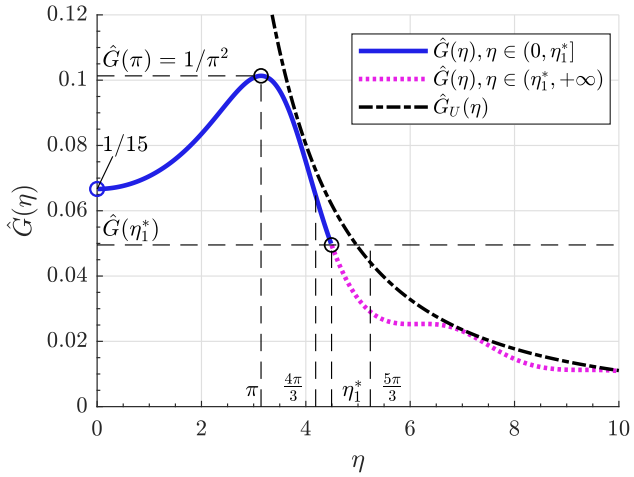

Figure 26: Illustration of the proof.

Because the boundary conditions are fixed, this function characterizes the magnitude of the cost, i.e. the best value of $\eta \in \mathcal{S}(C_0)$ is the one that provides the maximum to $\hat{G}(\eta)$. Therefore, it is sufficient to prove that

$$\hat{G}(\eta) \geq \hat{G}(\eta_1^*),\ \eta \in (0, \eta_1^*], \quad \hat{G}(\eta) < \hat{G}(\eta_1^*),\ \eta \in (\eta_1^*, \infty) \tag{A.24}$$

(i) By direct computation $\lim_{\eta\to 0} \hat{G}(\eta) = 1/15 \simeq 0.0667 > \hat{G}(\eta_1^*) \simeq 0.0495$.

(ii) Let us introduce a monotonically decreasing upper bound of $\hat{G}(\eta)$

$$\hat{G}_U(\eta) = \frac{1}{\eta^2}\frac{\eta + 1/2}{\eta - 1/2}, \quad \eta > 1/2 \tag{A.25}$$

which was obtained by bounding the terms of $\hat{G}(\eta)$ using $\eta\sin\eta\cos\eta \leq \eta/2$, $\sin^2\eta \geq 0$, and $\sin\eta\cos\eta \leq 1/2$. The upper bound assumes the value $\hat{G}(\eta_1^*)$ at the solution of the following cubic equation

$$\eta^3 - \frac{1}{2}\eta^2 - \hat{G}^{-1}(\eta_1^*)\eta - \frac{1}{2}\hat{G}^{-1}(\eta_1^*) = 0, \quad \eta > 1/2 \tag{A.26}$$

which is $\eta \simeq 4.9706 < 5\pi/3 \simeq 5.2360$. Hence,

$$\hat{G}(\eta) < \hat{G}(\eta_1^*),\ \eta \in (5\pi/3, \infty) \tag{A.27}$$

(iii) Let us take the derivatives of $\hat{G}(\eta)$ and $D(\eta)$

$$\hat{G}'(\eta) = \frac{2\,F(\eta)\sin\eta}{\eta^4\left(\eta - \sin\eta\cos\eta\right)^2} \tag{A.28}$$

$$D'(\eta) = -\frac{2\,F(\eta)\left(\sin\eta - \eta\cos\eta\right)}{\left(\eta^2 + 2\eta^2\cos^2\eta - 3\eta\sin\eta\cos\eta\right)^2} \tag{A.29}$$

where $F(\eta)$ is determined by Eq. (A.4). In Lemma 8 we proved that $F(\eta) > 0$ for $\eta \in (0, 5\pi/3)$. Then, $\hat{G}(\eta)$ is monotonically increasing on $\eta \in (0, \pi)$ and monotonically decreasing on $\eta \in (\pi, 5\pi/3)$.

From (i) – (iii) follows Eq. (A.24).

□

2. EOM Integration

For the convenience of the integration procedure, we introduce the following auxiliary result. Let $f(\sigma) \in \mathbb{R}$ be an integrable function on $\sigma \in [0,1] \subset \mathbb{R}$. Then

$$\int_0^t f\left(\tfrac{t_f-\xi}{t_f}\right)\,\mathrm{d}\xi = t_f\int_\tau^1 f(\sigma)\,\mathrm{d}\sigma \tag{B.1}$$

for all $t \in [0, t_f]$ and for all $\tau \in [0,1]$. Indeed, let $\tau = \frac{t_f-t}{t_f}$ and $\sigma = \frac{t_f-\xi}{t_f}$. So,

$$\int_0^t f\left(\tfrac{t_f-\xi}{t_f}\right)\,\mathrm{d}\xi = -t_f\int_0^t f\left(\tfrac{t_f-\xi}{t_f}\right)\,\mathrm{d}\left(\tfrac{t_f-\xi}{t_f}\right) = -t_f\int_1^\tau f(\sigma)\,\mathrm{d}\sigma = t_f\int_\tau^1 f(\sigma)\,\mathrm{d}\sigma \tag{B.2}$$

Now let us substitute Eq. (29) into Eq. (16) – Eq. (18) and perform the integration from 0 till $t \le t_f$. Let $\tau = \frac{t_f-t}{t_f}$. Then using the integration property above, the result is

$$x(t) = x_0 - Vt\left(1 - \frac{\theta_0^2}{2}\right) + \theta_0 K t_f^2\int_\tau^1 U(\eta,\sigma)\,\mathrm{d}\sigma + \frac{K^2t_f^3}{2V}\int_\tau^1 U^2(\eta,\sigma)\,\mathrm{d}\sigma \tag{B.3}$$

$$y(t) = y_0 - V\theta_0 t - Kt_f^2\int_\tau^1 U(\eta,\sigma)\,\mathrm{d}\sigma \tag{B.4}$$

$$\theta(t) = \theta_0 + \frac{Kt_f}{V}U(\eta,\tau) \tag{B.5}$$

where

$$U(\eta,\tau) \triangleq \int_\tau^1 u(\eta,\sigma)\,\mathrm{d}\sigma = \begin{cases} -\frac{1}{\eta^2}\left(\cos\eta - \cos\eta\tau\right), & \eta > 0 \\ \frac{1}{\eta^2}\left(\cosh\eta - \cosh\eta\tau\right), & \eta < 0 \\ \frac{1}{2}\left(1-\tau^2\right), & \eta = 0 \end{cases} \tag{B.6}$$

$$\int_\tau^1 U(\eta,\sigma)\,\mathrm{d}\sigma = \begin{cases} \frac{1}{\eta^3}\left(\sin\eta - \sin\eta\tau - \eta(1-\tau)\cos\eta\right), & \eta > 0 \\ -\frac{1}{\eta^3}\left(\sinh\eta - \sinh\eta\tau - \eta(1-\tau)\cosh\eta\right), & \eta < 0 \\ \frac{1}{2}\left(1-\tau-\frac{1}{3}\left(1-\tau^3\right)\right), & \eta = 0 \end{cases} \tag{B.7}$$

$$\int_\tau^1 U^2(\eta,\sigma)\,\mathrm{d}\sigma =$$

$$= \begin{cases} \frac{1}{2\eta^5}\left(\eta(1-\tau) + 2\eta(1-\tau)\cos^2\eta - \frac{3}{2}\sin 2\eta + 4\cos\eta\sin\eta\tau - \frac{1}{2}\sin 2\eta\tau\right), & \eta > 0 \\ \frac{1}{2\eta^5}\left(\eta(1-\tau) + 2\eta(1-\tau)\cosh^2\eta - \frac{3}{2}\sinh 2\eta + 4\cosh\eta\sinh\eta\tau - \frac{1}{2}\sinh 2\eta\tau\right), & \eta < 0 \\ \frac{1}{4}\left(\frac{8}{15} - \tau + \frac{2}{3}\tau^3 - \frac{1}{5}\tau^5\right), & \eta = 0 \end{cases} \tag{B.8}$$

Substituting $\tau = 0$ (equivalent to $t = t_f$) into Eq. (B.3) and Eq. (B.4), we obtain the terminal states as

$$x_f = x_0 - Vt_f\left(1 - \frac{1}{2}\theta_0^2\right) + \theta_0 K t_f^2 \int_0^1 U(\eta,\tau)\mathrm{d}\tau + \frac{K^2 t_f^3}{2V}\int_0^1 U^2(\eta,\tau)\mathrm{d}\tau \tag{B.9}$$

$$y_f = y_0 - Vt_f\theta_0 - Kt_f^2\int_0^1 U(\eta,\tau)\,\mathrm{d}\tau \tag{B.10}$$

where $\int_0^1 U(\eta,\tau)\,\mathrm{d}\tau$ and $\int_0^1 U^2(\eta,\tau)\mathrm{d}\tau$ are given by Eq. (40) and Eq. (41), respectively.

Using the initial condition $y_0 = 0$ and terminal conditions $x_f = 0$ and $y_f = 0$, and eliminating $\int_0^1 U(\eta,\tau)\,\mathrm{d}\tau$ in Eq. (B.9) with the help of Eq. (B.10), the system of equations Eq. (B.9)–Eq. (B.10) can be rearranged as Eq. (38) and Eq. (39).

References

[1] Zadka, B., Tripathy, T., Tsalik, R., and Shima, T., "Consensus-based cooperative geometrical rules for simultaneous target interception," *Journal of Guidance, Control, and Dynamics*, Vol. 43, No. 12, 2020, pp. 2425–2432.

[2] Merkulov, G., Weiss, M., and Shima, T., "Minimum-effort impact-time control guidance using quadratic kinematics approximation," *Journal of Guidance, Control, and Dynamics*, 2021, pp. 1–14.

[3] Jeon, I.-S., Lee, J.-I., and Tahk, M.-J., "Impact-time-control guidance law for anti-ship missiles," *IEEE Transactions on control systems technology*, Vol. 14, No. 2, 2006, pp. 260–266.

[4] Kumar, S. R. and Ghose, D., "Sliding mode control based guidance law with impact time constraints," *2013 American Control Conference*, IEEE, 2013, pp. 5760–5765.

[5] Cho, D., Kim, H. J., and Tahk, M.-J., "Nonsingular sliding mode guidance for impact time control," *Journal of Guidance, Control, and Dynamics*, Vol. 39, No. 1, 2015, pp. 61–68.

[6] Saleem, A. and Ratnoo, A., "Lyapunov-based guidance law for impact time control and simultaneous arrival," *Journal of Guidance, Control, and Dynamics*, Vol. 39, No. 1, 2015, pp. 164–173.

[7] Tekin, R., Erer, K. S., and Holzapfel, F., "Polynomial shaping of the look angle for impact-time control," *Journal of Guidance, Control, and Dynamics*, Vol. 40, No. 10, may 2017, pp. 2666–2671.

[8] Tekin, R., Erer, K. S., and Holzapfel, F., "Adaptive impact time control via look-angle shaping under varying velocity," *Journal of Guidance, Control, and Dynamics*, Vol. 40, No. 12, aug 2017, pp. 3247–3255.

[9] Tsalik, R. and Shima, T., "Circular Impact-Time Guidance," *Journal of Guidance, Control, and Dynamics*, 2019, pp. 1–12.

[10] Bruckstein, A. M., "Why the ant trails look so straight and nice," *The Mathematical Intelligencer*, Vol. 15, No. 2, 1993, pp. 59–62.

[11] Marshall, J. A., Broucke, M. E., and Francis, B. A., "Pursuit formations of unicycles," *Automatica*, Vol. 42, No. 1, 2006, pp. 3–12.

[12] Mallik, G. R., Daingade, S., and Sinha, A., "Consensus based deviated cyclic pursuit for target tracking applications," *Control Conference (ECC), 2015 European*, IEEE, 2015, pp. 1718–1723.

[13] Marshall, J. A., Broucke, M. E., and Francis, B. A., "Formations of vehicles in cyclic pursuit," *IEEE Transactions on automatic control*, Vol. 49, No. 11, 2004, pp. 1963–1974.

[14] Sinha, A. and Ghose, D., "Generalization of nonlinear cyclic pursuit," *Automatica*, Vol. 43, No. 11, 2007, pp. 1954–1960.

[15] Kumar, S. R. and Mukherjee, D., "Cooperative Salvo Guidance using Finite-Time Consensus over Directed Cycles," *IEEE Transactions on Aerospace and Electronic Systems*, 2019, pp. 1–1.

[16] Jadbabaie, A., Lin, J., and Morse, A. S., "Coordination of groups of mobile autonomous agents using nearest neighbor rules," *Proceedings of the 41st IEEE Conference on Decision and Control, 2002.*, Vol. 3, IEEE, 2002, pp. 2953–2958.

[17] Peng, K. and Yang, Y., "Leader-following consensus problem with a varying-velocity leader and time-varying delays," *Physica A: Statistical Mechanics and its Applications*, Vol. 388, No. 2-3, 2009, pp. 193–208.

[18] Zhu, W. and Cheng, D., "Leader-following consensus of second-order agents with multiple time-varying delays," *Automatica*, Vol. 46, No. 12, 2010, pp. 1994–1999.

[19] Shao, J., Xie, G., Yu, J., and Wang, L., "Leader-following formation control of multiple mobile robots," *Proceedings of the 2005 IEEE International Symposium on, Mediterrean Conference on Control and Automation Intelligent Control, 2005.*, IEEE, 2005, pp. 808–813.

[20] Consolini, L., Morbidi, F., Prattichizzo, D., and Tosques, M., "Leader–follower formation control of nonholonomic mobile robots with input constraints," *Automatica*, Vol. 44, No. 5, 2008, pp. 1343–1349.

[21] Sun, X., Zhou, R., Hou, D., and Wu, J., "Consensus of leader-followers system of multi-missile with time-delays and switching topologies," *Optik-International Journal for Light and Electron Optics*, Vol. 125, No. 3, 2014, pp. 1202–1208.

[22] Rudin, W. et al., *Principles of mathematical analysis*, Vol. 3, McGraw-hill New York, 1964.

[23] Bressan, A. and Piccoli, B., *Introduction to the mathematical theory of control*, Vol. 1, American institute of mathematical sciences Springfield, 2007.

[24] Ben-Asher, J. Z., *Optimal Control Theory with Aerospace Applications (AIAA Education Series)*, AIAA education series, American Institute of Aeronautics and Astronautics, Reston, Va, 2009.

[25] Chen, Z. and Shima, T., "Nonlinear optimal guidance for intercepting a stationary target," *Journal of Guidance, Control, and Dynamics*, Vol. 42, No. 11, 2019, pp. 2418–2431.

[26] Jeon, I. S., Lee, J. I., and Tahk, M. J., "Impact-time-control guidance law for anti-ship missiles," *IEEE Transactions on Control Systems Technology*, Vol. 14, No. 2, 2006, pp. 260–266.

[27] Ryoo, C. K., Cho, H., and Tahk, M. J., "Optimal guidance laws with terminal impact angle constraint," *Journal of Guidance, Control, and Dynamics*, Vol. 28, No. 4, may 2005, pp. 724–732.

[28] N.A. Shneydor, *Missile Guidance and Pursuit: Kinematics, Dynamics and Control*, Elsevier, 1998.

[29] Rieck, M., Bittner, M., Grüter, B., Diepolder, J., and Piprek, P., *FALCON.m User Guide*, Institute of Flight System Dynamics, Technical University of Munich, 2019.

[30] Zarchan, P., *Tactical and Strategic Missile Guidance, Sixth Edition*, American Institute of Aeronautics and Astronautics, Inc., 2012.

[31] Bronshtein, I. N., Semendyayev, K. A., Musiol, G., and Mühlig, H., *Handbook of Mathematics*, Springer Berlin Heidelberg, Berlin, Heidelberg, 4th ed., 2004.

[32] Biernacki, M. and Krzyż, J., "On the monotonity of certain functionals in the theory of analytic functions," *Annales Universitatis Mariae Curiae-Skłodowska, Sectio A, Mathematica*, Vol. 9, 1955, pp. 5–23.